Control of protein synthesis and memory by GluN3A-NMDA receptors through inhibition of GIT1/mTORC1 assembly

María J. Conde-Dusman[1,2§], Partha N. Dey[2†§], Oscar Elía-Zudaire[1§], Luis G. Rabaneda[1,2‡], Carmen García-Lira[1], Teddy Grand[3], Victor Briz[4], Eric R. Velasco[5,6], Raúl Andero[5,6], Sergio Niñerola[1], Angel Barco[1], Pierre Paoletti[3], John F. Wesseling[1], Fabrizio Gardoni[7], Steven J. Tavalin[8] and Isabel Pérez-Otaño[1,2]*

[1] Instituto de Neurociencias (CSIC-UMH), San Juan de Alicante 03550, Spain.
[2] Centro de Investigación Médica Aplicada (CIMA), University of Navarra, Pamplona 31008, Spain.
[3] Institut de Biologie de l'Ecole Normale Supérieure (IBENS), Ecole Normale Supérieure, Université PSL, CNRS, INSERM, Paris F-75005, France.
[4] Centro de Biología Molecular Severo Ochoa (UAM-CSIC), Madrid 28049, Spain.
[5] Institut de Neurociències and Departament de Psicobiologia i de Metodologia de les Ciències de la Salut, Universitat Autònoma de Barcelona, 08193 Bellaterra, Spain.
[6] Centro de Investigación Biomédica en Red de Salud Mental (CIBERSAM), Carlos III Health Institute, 28029 Madrid, Spain.
[7] Department of Pharmacological and Biomolecular Sciences, University of Milan, Milan 20133, Italy.
[8] Department of Pharmacology, Addiction Science, and Toxicology, College of Medicine, University of Tennessee Health Science Center, Memphis, Tennessee 38103, USA.

Current address: [†]National Eye Institute, National Institutes of Health, Bethesda, MD, USA; ‡ Institute of Science and Technology Austria (IST), Klosterneuburg, Austria.

[§] These authors contributed equally to this work.

* Correspondence should be addressed to *otano@umh.es*

Short title: Synaptic control of translation and memory by GluN3A/GIT1

ABSTRACT

De novo protein synthesis is required for synapse modifications underlying stable memory encoding. Yet neurons are highly compartmentalized cells and how protein synthesis can be regulated at the synapse level is unknown. Here we characterize neuronal signaling complexes formed by the postsynaptic scaffold GIT1, the mTOR kinase and Raptor that couple synaptic stimuli to mTOR-dependent protein synthesis; and identify NMDA receptors containing GluN3A subunits as key negative regulators of GIT1 binding to mTOR. Disruption of GIT1/mTOR complexes by enhancing GluN3A expression or silencing GIT1 inhibits synaptic mTOR activation and restricts the mTOR-dependent translation of specific activity-regulated mRNAs. Conversely, GluN3A removal enables complex formation, potentiates mTOR-dependent protein synthesis, and facilitates the consolidation of associative and spatial memories in mice. The memory enhancement becomes evident with light or spaced training, can be achieved by selectively deleting GluN3A from excitatory neurons during adulthood, and does not compromise other aspects of cognition such as memory flexibility or extinction. Our findings provide mechanistic insight into synaptic translational control and reveal a potentially selective target for cognitive enhancement.

Keywords

NMDA receptors, synapse, translation, mTOR, GIT1, long-term memory, *Grin3a*

INTRODUCTION

Brains are made of complex neuronal networks and memories are encoded by modifying the synaptic connections between them. Encoding requires *de novo* mRNA and protein synthesis in response to neuronal activity and sensory experience. It entails the transcription of immediate early genes (IEGs) to mRNA, and the protein products of some IEG transcripts mediate structural and functional modifications of synapses (Yap and Greenberg, 2018). However, transcription occurs in the cell body and generates a neuron-wide pool of mRNAs, whereas only a fraction of synapses of any individual neuron are modified by a given memory (Holtmaat and Caroni, 2016; Josselyn and Tonegawa, 2020). To ensure input specificity, transcription is coupled to local mechanisms that restrict the effects of activity-induced gene products to selected synapses (Wang et al., 2010).

One of these mechanisms is thought to be the local, synapse-specific translation of mRNA into protein (Holt et al., 2019; Klann and Dever, 2004; Sossin and Costa-Mattioli, 2019). The main rate-limiting step in translation is initiation, which is regulated by the phosphorylation of two separate proteins: the eukaryotic initiation factor 2α (eIF2α) and the mTOR ("mechanistic target of rapamycin") serine/threonine kinase. Manipulations of eIF2α phosphorylation have been implicated in synapse plasticity and memory, but eIF2α affects general mRNA translation and evidence for a role in local translation is lacking (Sharma et al., 2020; Shrestha et al., 2020b). mTOR could in principle afford more selective translational control. mTOR forms at least two distinct multiprotein complexes, mTORC1 and mTORC2. mTORC1 is defined by the presence of Raptor, an adaptor protein which recruits mTOR substrates to promote the translation of specific mRNAs, and compartmentalized activation has been shown to be essential for mTORC1 responses to nutrients in non-neuronal cells (Liu and Sabatini, 2020). In neurons, components of mTORC1 localize to axons, dendrites and synapses (Poulopoulos et al., 2019; Takei et al., 2004; Tang et al., 2002), and pharmacological inhibition of mTORC1 with rapamycin blocks long-lasting synaptic plasticity and memory formation (Cammalleri et al., 2003; Hou and Klann, 2004; Stoica et al., 2011; Tang et al., 2002). Moreover, dysregulated translation is a feature in diseases of cognition, from autism to intellectual disability, and many of the mutations associated with these diseases affect genes encoding negative regulators of mTORC1 (Costa-Mattioli and Monteggia, 2013; Lipton and Sahin, 2014). However, it is currently unclear how mTOR activation might be controlled at specific synapses and linked to mechanisms that gate learning and memory.

The most intensively studied mechanism gating learning and memory involves the NMDA-type glutamate receptor (NMDAR). NMDARs contain multiple subunits, including an obligatory GluN1 subunit, various GluN2 (A-D) and, for some subtypes, one of the GluN3 (A-B) subunits (Paoletti et al., 2013). Conventional subtypes containing GluN1 and GluN2 trigger gene expression programs that mediate the strengthening and stabilization of active synapses and the persistent storage of information (Lyons and West, 2011). By contrast, non-conventional subtypes containing the GluN3A

subunit (GluN3A-NMDARs) inhibit many of these synaptic modifications (Perez-Otano et al., 2016). Synapses that express GluN3A are resistant to the induction of long-lasting functional and structural plasticity, and memories fade more quickly in mutant mice with enhanced GluN3A expression (Kehoe et al., 2014; Roberts et al., 2009). In line with this work in mice, human genetic studies correlate enhanced cognitive performance with low GluN3A levels or variations in *GRIN3A* (human gene encoding GluN3A) (Gallinat et al., 2007; Papenberg et al., 2014; Sadat-Shirazi et al., 2019); and GluN3A dysregulation in humans is linked to cognitive impairment in schizophrenia (Greenwood et al., 2019; Mueller and Meador-Woodruff, 2004; Ohi et al., 2015; Takata et al., 2013), Huntington disease (Marco et al., 2013), addiction and other pathologies (Huang et al., 2017; Perez-Otano et al., 2016; Sarker et al., 2019; Yang et al., 2015; Yuan et al., 2013). We reasoned that understanding the underlying mechanisms would yield insight into the brain processes that constrain long-term memory formation and might uncover targets for therapeutic intervention.

Here we report that GluN3A-NMDARs selectively and negatively regulate synaptic mTORC1-dependent translation without affecting neuron-wide transcriptional activation. Negative regulation is mediated by inhibition of the assembly of mTORC1 complexes that contain the postsynaptic adaptor GIT1 (G protein-coupled receptor kinase-interacting protein) and Raptor, are located at or near synaptic sites, and couple mTORC1 kinase activity to synaptic stimulation. Through biochemical, mouse genetics and behavioral approaches, we further show that GluN3A deletion increases the availability of GIT1/mTORC1 complexes, boosts mTORC1-dependent protein synthesis, and facilitates long-term memory formation. The advantage is selectively evident when mice are subjected to weak training behavioral paradigms; can be reversed by the mTORC1 inhibitor rapamycin; and unlike the memory enhancement seen after manipulations of general translational regulators, is not associated with deficits in memory flexibility or extinction (Shrestha et al., 2020a). Our findings identify a novel regulatory mechanism whereby GluN3A/GIT1 interactions set local modes of protein synthesis and gate memory formation, and reveal a potentially selective target for correcting cognitive impairment in pathological contexts.

RESULTS

Selective inhibition of activity-dependent gene expression by GluN3A at the post-transcriptional level

GluN3A expression is pervasive during postnatal brain development, and regulated removal allows for the activity-dependent stabilization or elimination of excess synapses (Perez-Otano et al., 2016). To assess whether GluN3A-NMDARs modulate activity-dependent gene expression, we expressed GluN3A in cultured cortical neurons over the stage when endogenous down-regulation normally occurs (days *in vitro* (DIV) 9-14, ~postnatal days P8-P16 *in vivo*, Figure 1A – figure supplement 1A)(Kehoe et al., 2014). We used lentiviral vectors where expression is targeted to neurons by the synapsin 1 promoter and induced synaptic activity with bicuculline, which inhibits ɣ-aminobutyric acid (GABA) transmission and triggers bursts of action potential firing (Hardingham et al., 2002).

As expected, bicuculline induced a robust expression of immediate-early genes (IEGs) implicated in the consolidation of synaptic modifications and memories, including Arc, c-Fos and Zif268/Egr1 (Flavell and Greenberg, 2008) (Figure 1B). Enhancing GluN3A expression largely reduced the induction of Arc and c-Fos proteins while Zif268 induction was unaffected, indicating that GluN3A selectively inhibits specific activity-dependent signaling pathways (Figure 1B). Analysis at the mRNA level demonstrated that modulation occurs downstream of gene transcription: *Arc, c-Fos* and *Zif268* mRNA levels were strongly induced by bicuculline in both control and GluN3A-infected neurons, and no differences were observed in the time-courses or magnitude of induction (Figure 1C). Unchanged transcription was in-line with intact activation of the phosphorylation of extracellular signal-regulated kinase (ERK1/2) and CREB (Figure 1 – figure supplement 1B), the two major pathways for activity-dependent transcription (Flavell and Greenberg, 2008). By contrast, the general NMDAR antagonist D-2-amino-5-phosphonovaleric acid (APV) inhibited all signaling pathways analyzed and the induction of IEGs at both mRNA and protein levels (Figure 1 – figure supplement 1C, D).

An analogous dissociation between protein and transcript levels of a subset of IEGs (Figure 1 – figure supplement 1E, F) was observed when GluN3A-infected neurons were stimulated with the neurotrophin BDNF, a potent inducer of gene expression at both transcriptional and translational levels (Rao et al., 2006). Whole transcriptome RNAseq analyses confirmed that transcriptional responses to bicuculline or BDNF were unaffected by GluN3A expression (Figure 1D; Figure 1 – figure supplement 2). Together these results indicated that GluN3A-NMDARs repress the translation of specific activity-regulated mRNAs without affecting global transcriptional programs of gene expression. Inhibited induction of IEGs by GluN3A was not rescued by pre-treatment with the proteasome inhibitor MG-132 (Figure 1E), ruling out alternative mechanisms such as enhanced proteasome-dependent degradation (Rao et al., 2006).

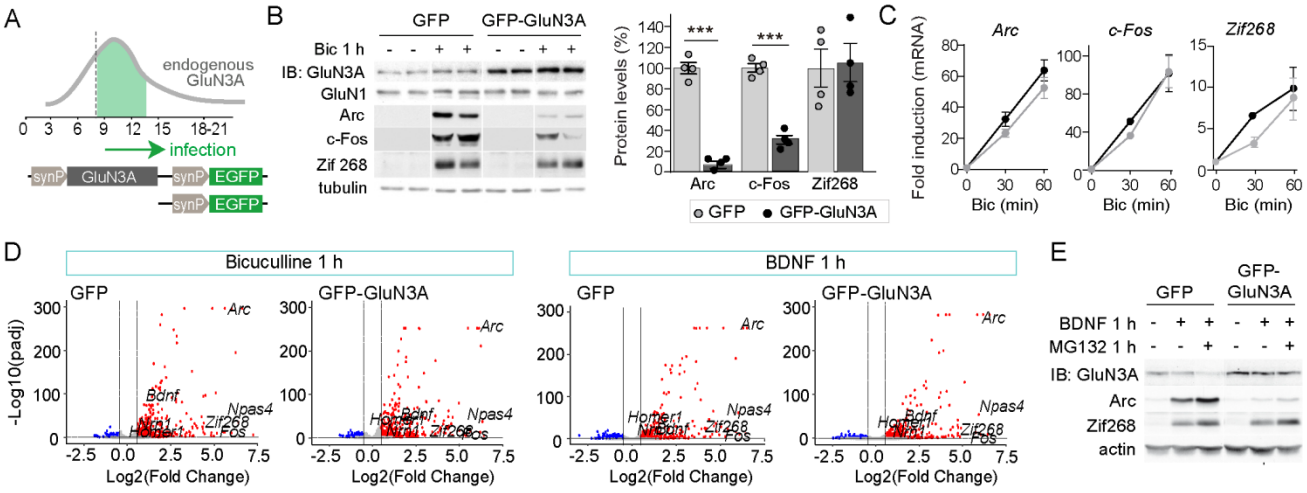

Figure 1. **GluN3A inhibits the activity-dependent induction of a subset of IEGs**

(A) Timeline of endogenous GluN3A expression and down-regulation and of lentiviral infections. Cortical neurons in primary culture were infected on DIV9 with lentiviruses where GFP or GluN3A and GFP (GFP-GluN3A) expression is driven by the human synapsin 1 promoter (synP). **(B, C)** DIV14 neurons were treated with bicuculline (50 µM, 1 h) and matching samples collected for immunoblot and mRNA analyses (n=4 from 2 independent cultures; ***p<0.001, two-tailed unpaired t-test). **(B)** Left, representative western blots show that GluN3A inhibits the induction of the immediate early genes (IEGs) Arc and c-Fos but not Zif268. Right, signal intensities of indicated proteins as percentage of stimulated GFP-infected neurons. **(C)** qRT-PCR analysis of IEG mRNA induction. Plotted values are fold-induction relative to non-stimulated neurons. **(D)** Volcano plots presenting the RNAseq-based differential expression analysis in DIV14 neurons treated with bicuculline or BDNF for 1h (n=2-4 from 2 independent cultures). **(E)** DIV14 neurons were treated with MG132 (30 µM). A representative western blot probed with the indicated antibodies is shown. In immunoblot analyses, tubulin or actin was used as a loading control and GluN1 as a measure of potential effects of GluN3A on overall NMDAR numbers. Histograms in this and subsequent figures are mean ± s.e.m.

Figure 1 – figure supplement 1. Selective *versus* global effects of GluN3A expression and general NMDAR blockade on activity-dependent signaling

Figure 1 – figure supplement 2. RNAseq analysis of activity-dependent gene expression

GluN3A inhibits mTORC1-dependent translation of IEGs

We thus turned to protein synthesis pathways to search for mechanisms underlying the selective inhibition of gene expression by GluN3A. We focused on mTORC1 because it has been shown to couple synaptic signals including BDNF and NMDAR activation to translation of specific mRNAs in dendrites and synapses (Takei et al., 2004; Tang et al., 2002). mTORC1 signaling was strongly activated by bicuculline in DIV14 cortical neurons, as shown by phosphorylation of mTOR on Ser^{2448} (a reliable readout of mTORC1 kinase activity; see Chiang and Abraham, 2005) and of its downstream effectors, the p70-kDa ribosomal protein S6 kinase (S6K, Thr^{389}) and ribosomal protein S6 (Ser^{240-4}, Figure 2A, B). The effects were blocked by APV and the NMDAR open-channel blocker MK-801, confirming NMDAR-dependence in our model (Figure 2 - figure supplement 1A).

Phosphorylation of mTOR, S6K and S6 following bicuculline treatment was significantly reduced in GluN3A-infected neurons, indicating that GluN3A interferes with synaptic mTORC1 activation (Figure 2B). Two experiments linked mTORC1 inhibition to the altered production of IEGs (Figure 2 - figure supplement 1B). First, low concentrations of rapamycin (100 nM) that inhibit mTORC1 but not mTORC2 (Zhu et al., 2018), blocked Arc and c-Fos translation in response to bicuculline without affecting Zif268, demonstrating selective mTORC1-dependence. By contrast, the general protein synthesis inhibitor anisomycin fully suppressed Arc, c-Fos and Zif268 induction (Figure 2 - figure supplement 1C). Second, restoring mTORC1 signaling in GluN3A-infected neurons by expressing a constitutively active form of Rheb, the main upstream activator of mTORC1, was sufficient to normalize IEG induction (Figure 2 - figure supplement 1D).

Conversely, lentiviral knockdown of GluN3A in cortical neurons with a validated short hairpin RNA (Kehoe et al., 2014) enhanced mTORC1 activity (Figure 2C, D) and potentiated the induction of Arc and c-Fos by bicuculline or BDNF (Figure 2E, F). Increased phosphorylation of S6K and S6 was additionally detected in hippocampal lysates from mice lacking GluN3A (*Grin3a*-/-) relative to wild-type littermates (Figure 2G), confirming a role of GluN3A in limiting mTORC1 signaling *in vivo*.

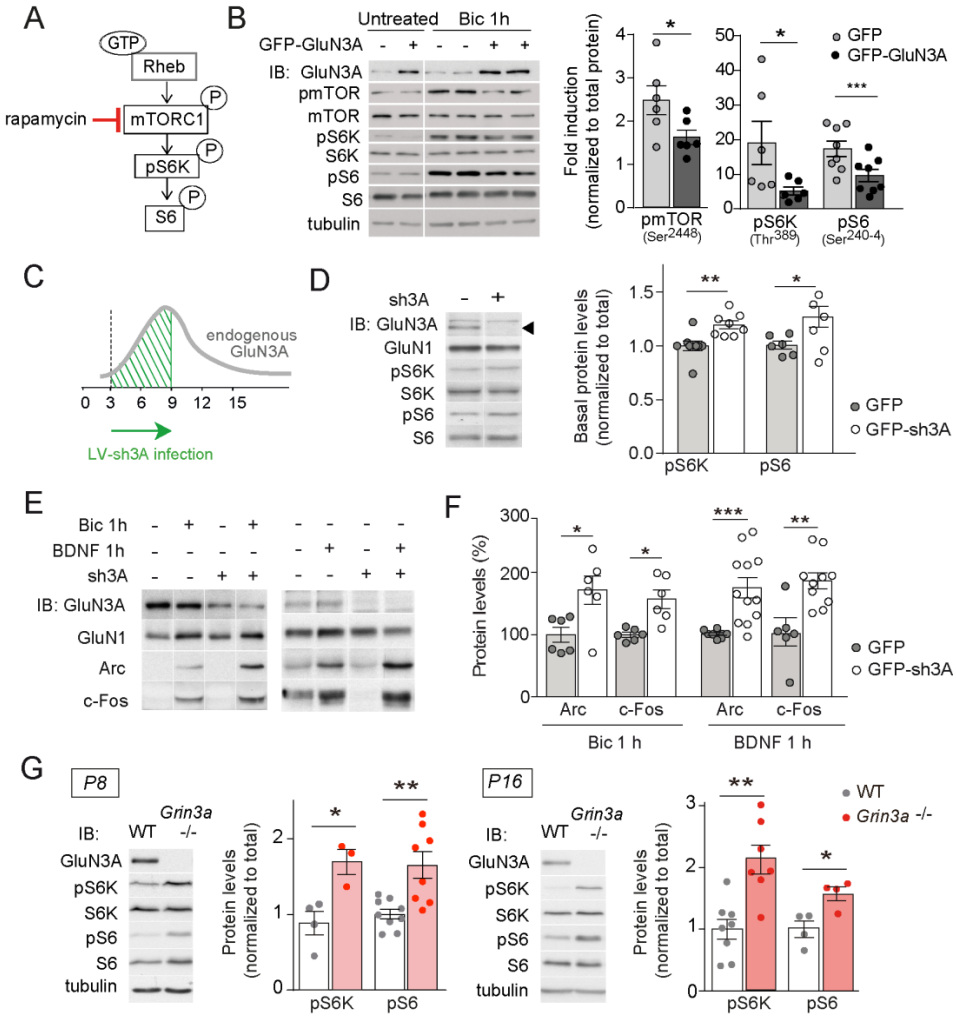

Figure 2. GluN3A expression regulates synaptic mTORC1 activation

(A) Schematic of the mTORC1 signaling pathway. **(B)** Left, representative western blots of cortical neurons infected with GFP and GFP-GluN3A (DIV9) and treated with bicuculline at DIV14. Right, fold-induction of phosphorylated mTOR, S6K and S6 normalized to total protein (n=6-8 from 3-4 independent cultures; *p<0.05, ***p<0.001, two-tailed paired t-test). **(C-F)** Neurons were infected on DIV3 with lentiviruses expressing GFP alone or along with a shRNA against GluN3A (GFP-sh3A) and collected at DIV7-9, when GluN3A expression is maximal. **(D)** Representative blots and quantification of phosphorylated S6K and S6

normalized to total protein (n=6-8 from 3-4 independent cultures; *p<0.05, **p<0.01 two-tailed paired t-test). Arrow marks specific GluN3A band. **(E, F)** Representative western blots and quantification of IEG induction by bicuculline or BDNF (n=6-12 from 3 independent cultures; *p<0.05, **p<0.01, ***p<0.001, two-tailed paired t-test). Data plotted as percentage of stimulated control GFP-infected neurons**. (G)** Immunoblots and quantification of S6K and S6 phosphorylation in lysates from wild-type (WT) and *Grin3a-/-* hippocampi (n=4-8 mice; *p<0.05, **p<0.01, two-tailed unpaired t-test).

Figure 2 – figure supplement 1. Selective mTORC1-dependence of IEG translation

mTORC1 inhibition requires GluN3A C-terminal domain interactions

GluN3A subunits confer unique biophysical properties to NMDARs, including reduced channel conductance and calcium permeability, and enable distinct interactions with signaling/scaffolding proteins via their intracellular C-terminal tail (Perez-Otano et al., 2016). To dissect their contribution to inhibited mTORC1 signaling, we derived primary cortical neurons from *Grin3a-/-* mice and re-expressed full-length GluN3A, a mutant where the distal 33 amino acids of the GluN3A C-terminus have been deleted and lacks synapse destabilizing activity (GluN3A1082Δ) (Fiuza et al., 2013; Kehoe et al., 2014), or GFP as a control (Figure 3A). While full-length GluN3A rescued the enhanced mTOR activation and hyper-induction of Arc and c-Fos proteins by bicuculline or BDNF in *Grin3a-/-* cultures, the GluN3A1082Δ mutant failed to do so (Figure 3B-E). Neither GluN3A nor GluN3A1082Δ modified the activation of other signaling pathways such as ERK1/2 phosphorylation or the induction of Zif268 in *Grin3a-/-* neurons (Figure 3D).

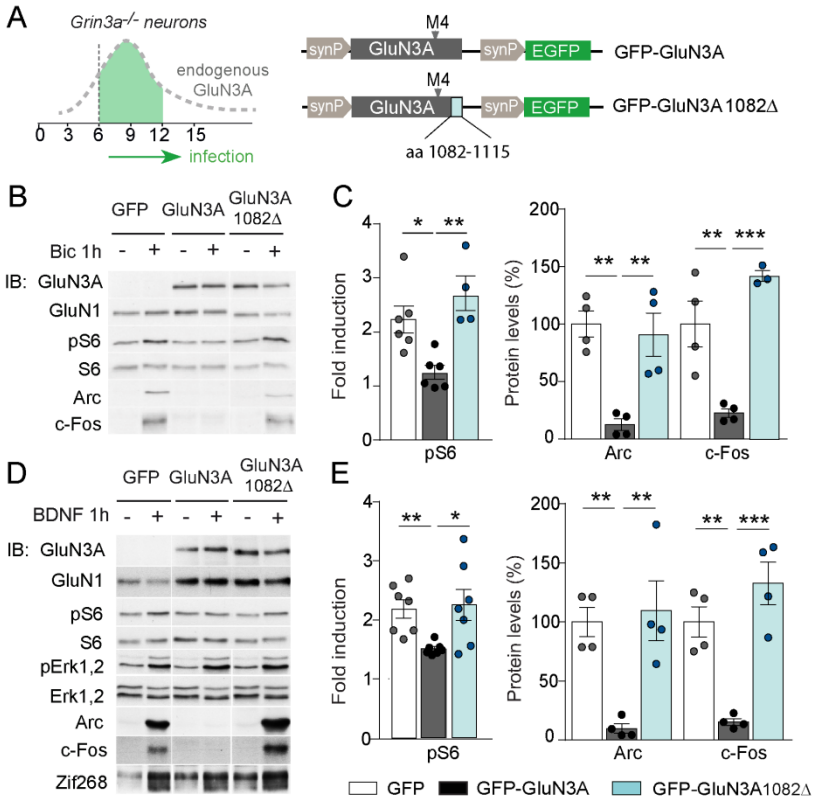

Figure 3. mTORC1 inhibition is mediated by GluN3A C-terminal domain interactions

(A) Cortical neurons from *Grin3a-/-* mice were infected on DIV6 with lentiviruses expressing GFP, GFP-GluN3A or GFP-GluN3A1082Δ, and stimulated with bicuculline or BDNF at DIV12. **(B, D)** Representative western blots of lysates from bicuculline or BDNF-treated neurons probed for the indicated antibodies. **(C, E)** Induction of phosphorylated S6 (normalized to total levels), Arc and c-Fos by bicuculline (n=3-7 from 2-4 independent cultures, *p<0.05, **p<0.01, ***p<0.001 ANOVA followed by Tukey's test).

Figure 3 – figure supplement 1. Electrophysiological properties of recombinant NMDA and excitatory glycine receptors containing full-length or truncated GluN3A

Since GluN3A and GluN3A1082Δ display similar distributions and cell surface targeting (Fiuza et al., 2013), the differences we observed are unlikely to stem from altered subcellular localization. We evaluated whether the deletion alters ion fluxes via GluN3A-NMDARs by analyzing electrophysiological responses to glutamate of GluN3A and GluN3A1082Δ co-expressed with GluN1 and GluN2A in HEK293 cells. The relative calcium permeability was estimated by measuring the shift in reversal potential (ΔE_{rev}) of recombinant NMDAR currents induced by changing extracellular Ca^{2+} (Perez-Otano et al., 2001). GluN3A and GluN3A1082Δ yielded similarly reduced shifts in ΔE_{rev} relative to conventional GluN1/GluN2A NMDARs, confirming that the mutant incorporated into functional triheteromeric GluN3A-NMDARs and arguing against differences in Ca^{2+} permeability (Figure 3 - figure supplement 1A). In addition, both GluN3A versions drove comparable reductions in current densities relative to conventional NMDARs (Figure 3 - figure supplement 1B). Along with non-conventional NMDARs, GluN3A subunits can form glycine-gated diheteromeric GluN1/GluN3 receptors (Perez-Otano et al., 2016). Thus we additionally examined whether the deletion modified responses to glycine of GluN1/GluN3 receptors taking advantage of the CGP-78608 compound (Grand et al., 2018) (Figure 3 - figure supplement 1C), but no differences were found. The absence of ionotropic differences favored the hypothesis that inhibition of mTOR signaling requires metabotropic interactions of GluN3A-NMDARs, possibly modulating its association with synaptic adaptors or scaffolds.

GluN3A expression modulates the assembly of synaptic GIT1/mTORC1 complexes

A leading candidate is the multifunctional adaptor GIT1. GIT1 is enriched in postsynaptic compartments and binds the 33 amino acids of the GluN3A C-terminus that we show above are required for mTORC1 inhibition (Fiuza et al., 2013). Although best known for its role in actin signaling (Zhang et al., 2003), GIT1 has been detected in mTOR immunoprecipitates from mouse astrocytes by mass spectrometry (Smithson and Gutmann, 2016) though a function for this association could not be established. Using reciprocal immunoprecipitation with GIT1 and mTOR antibodies, we isolated GIT1/mTOR complexes from lysates of microdissected hippocampal (Figure 4A) and cortical (not shown) tissue. We chose detergent conditions that preserve mTOR interactions with Raptor and Rictor (0.3% CHAPS) to further characterize the composition of the complex, and were able to identify Raptor (but not the mTORC2 component Rictor) in GIT1 immunoprecipitates. The mTOR antibody pulled-down both, validating our assay conditions (Figure 4A). The GIT1-binding protein and Rac1 activator ßPIX was also pulled down by the mTOR antibody while the control presynaptic protein synaptophysin was not (Figure 4A). We additionally

detected phosphorylated mTOR at Ser^{2448} in GIT1 immunoprecipitates, demonstrating GIT1/mTORC1 complex functionality (Figure 4B).

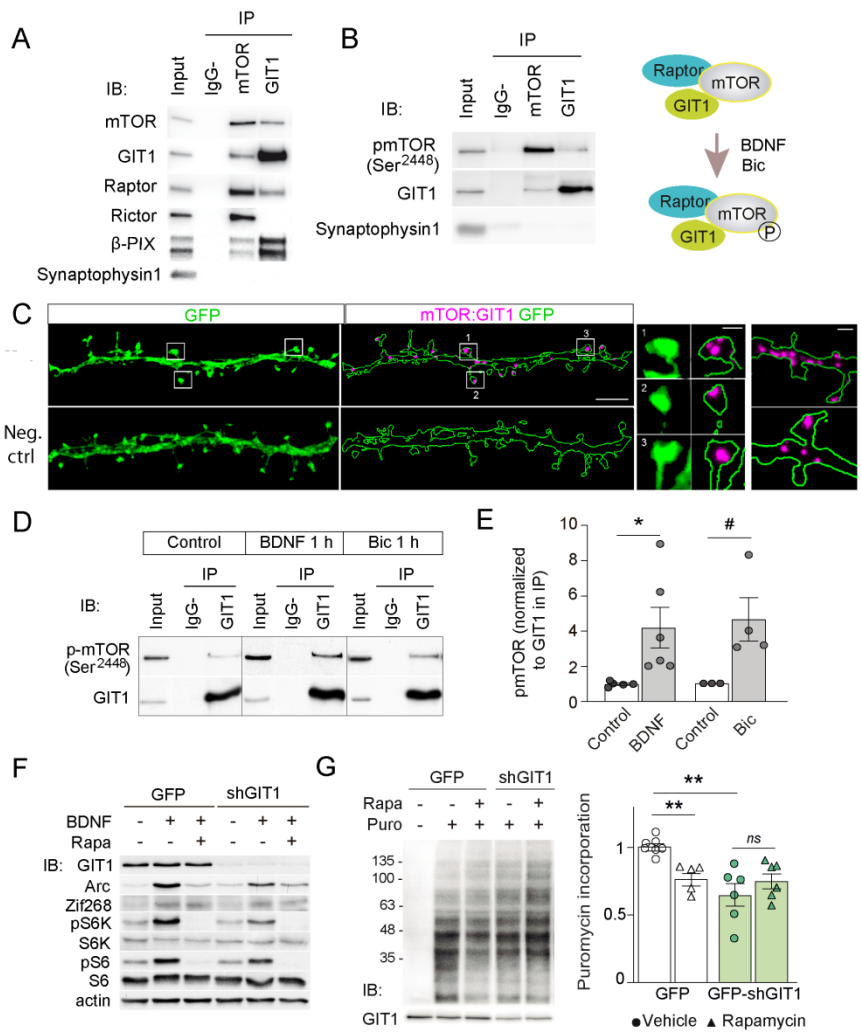

Figure 4. GIT1/mTOR/Raptor complexes couple synaptic activation to mTORC1-dependent protein synthesis

A, B) Protein extracts from P16 mouse hippocampus were solubilized with 0.3% CHAPS buffer, incubated with antibodies against mTOR or GIT1 (IP), and immunoprecipitated proteins analysed by immunoblot (IB). Input: 10% of the lysate used for immunoprecipitation. IgG-: no antibody control. A cartoon of the interactions and regulation by activity (see panel **D**) is shown. **(C)** Representative images of proximity ligation assay for mTOR: GIT1 (magenta) in DIV17 hippocampal neurons transfected with GFP (green) to visualize dendritic morphology (scale bar, 5 µm). High magnification examples of spines (scale bar, 0.5 µm) and dendrites (scale bar, 1 µm) are shown. As negative control, only mTOR primary antibody was used. **(D, E)** Cortical neurons stimulated with BDNF or bicuculline were solubilized with 0.3% CHAPS and incubated with GIT1 antibody (IP). Representative immunoblots (D) and quantification of mTOR phosphorylation in GIT1 immunoprecipitates (E) are shown (n=3-6 from 3 independent cultures; *p<0.05, #=0.06, two-tailed unpaired t-test). **(F, G)** Cortical neurons were infected with lentiviruses expressing GFP or GFP-shGIT1, and responses to BDNF **(F)** and puromycin incorporation in the presence or absence of 100 nM rapamycin **(G)** were analyzed at DIV14 (n=5-7 from 4 independent cultures, **p<0.01, two-way ANOVA followed by Tukey's test). Puromycin levels were normalized to Ponceau S staining.

Figure 4 – figure supplement 1. GIT1 knockdown reduces mTORC1 activation by BDNF and rapamycin-sensitive Arc translation

We then examined the subcellular localization of GIT1/mTORC1 complexes using *in situ* proximity-ligation assay (PLA) with antibodies against GIT1 and mTOR. PLA puncta were present along dendritic shafts often localized within or at the base of dendritic spines (Figure 4C), suggesting that GIT1 positions mTORC1 near synaptic sites to mediate dendritic translation in response to synaptic signals. To test this, we stimulated cortical neurons with bicuculline or BDNF

and quantified mTOR phosphorylation in total lysates and GIT1 immunoprecipitates. Both bicuculline and BDNF induced large increases in the phosphorylation of GIT1-bound mTOR on Ser^{2448} (Figure 4D, E). Importantly, the phosphorylation of GIT1-bound mTOR was much higher than phosphorylation of the total cellular mTOR pool (BDNF: 1.98 ± 0.38-fold increase in total lysates *vs* 4.2 ± 1.15 in GIT1-immunoprecipates; bicuculline: 1.42 ± 0.15 *vs* 4.63 ± 1.24), consistent with a role for GIT1 in nucleating synaptic mTORC1 activation. Further evidence came from GIT1 loss-of-function experiments. Lentiviral knockdown of GIT1 blunted the activation of mTORC1 by BDNF, as shown by reduced phosphorylation of S6 and S6K (Figure 4F; Figure 4- supplement 1A), and inhibited mTORC1-dependent protein synthesis assessed using a non-radioactive puromycin-labeling assay (SUnSET) (Figure 4G). Arc translation was also reduced, as judged by loss of rapamycin sensitivity relative to control neurons, while Zif268 which is mTORC1-independent was unaffected (Figure 4F; Figure 4 - figure supplement 1B). Collectively, these experiments demonstrated the existence of mTORC1 complexes composed of GIT1, mTOR and Raptor that mediate mTORC1 signaling in response to synaptic stimuli.

GluN3A/GIT1 interactions control the emergence of mTORC1-dependent protein synthesis

We further found that the abundance of GIT1/mTORC1 complexes is regulated throughout postnatal development. GIT1/mTORC1 complexes were readily observed in P16, but not P7 or P10, hippocampus or cortex of wild-type mice (Figure 5A; Figure 5 - figure supplement 1). Because this time-course matches well the timing of synaptic GluN3A down-regulation *in vivo* (Henson et al., 2012), we asked whether GluN3A expression influences GIT1/mTORC1 assembly. Biochemical analysis of GIT1 immunoprecipitates from hippocampi of P10 wild-type and *Grin3a*-/- showed that GluN3A removal enables the formation of GIT1/mTORC1 complexes at earlier stages, as judged by enhanced GIT1/mTOR and GIT1/Raptor binding (Figure 5B). Reciprocally, re-expression of full-length GluN3A (but not the GluN3A1082Δ mutant) in *Grin3a*-/- neurons was sufficient to prevent the GIT1/mTOR association, indicating that GluN3A-bound GIT1 cannot incorporate into the complex (Figure 5C). Taken together, the results support a model where GluN3A expression regulates the abundance of synaptic GIT1/mTORC1 complexes by directly binding GIT1, impeding its association with mTOR and limiting mTORC1 activation and downstream protein synthesis of plasticity factors. Conversely, developmental or genetic GluN3A down-regulation enables GIT1/mTORC1 formation and primes synapses for mTORC1-dependent translation (Figure 5D).

To test this model, we asked whether genetic manipulations of GluN3A/GIT1 interactions affect the timing and magnitude of mTORC1-dependent protein synthesis. A first set of experiments showed that protein synthesis in young cortical neurons (DIV7-9) is not dependent on mTORC1 activation, with strong rapamycin sensitivity emerging at later stages (DIV14; Figure 5 - figure supplement 2). Knockdown of GluN3A resulted in a large increase in protein synthesis in DIV7-9

neurons, which exhibited a rapamycin-dependence typical of mature neurons (Figure 5E). Robust rapamycin-dependent protein synthesis was also observed in *Grin3a-/-* neurons (Figure 5F). Re-expression of GluN3A, but not GluN3A1082Δ, reduced protein synthesis rates and was sufficient to block mTORC1-dependence, reinstating a juvenile mode of protein synthesis (Figure 5F). Thus GluN3A, via binding to GIT1, controls the age-dependent switch between mTORC1-independent and mTORC1-dependent protein synthesis.

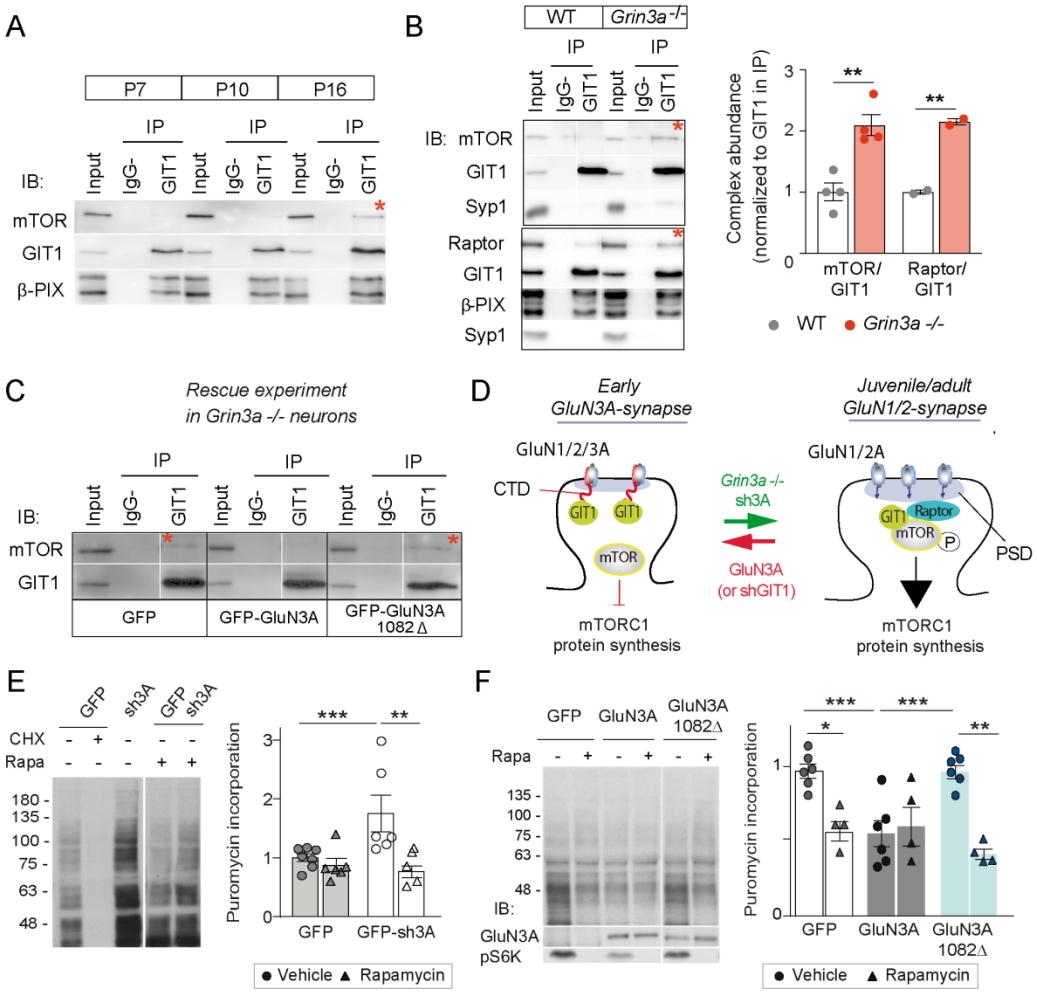

Figure 5 GluN3A/GIT1 interactions control the age-dependent onset of mTORC1-dependent protein synthesis

(A) Hippocampi from P7, P10 and P16 wild-type mice were lysed, immunoprecipitated with GIT1 antibody and probed for the indicated antibodies. Input: 10% of the lysate used for immunoprecipitation. IgG-: negative control without antibody. Red asterisks here and other panels indicate mTOR- and Raptor bound to GIT1. **(B)** GIT1/mTORC1 complex formation is enhanced in P10 *Grin3a-/-* hippocampus. Representative blots of GIT1 immunoprecipitates and quantifications are shown (n=2-4 mice; **p<0.01 unpaired t-test). Bound mTOR and Raptor are normalized to immunoprecipitated GIT1. Syp1: synaptophysin 1 **(C)** *Grin3a-/-* cortical neurons infected with GFP, GFP-GluN3A or GFP-GluN3A1082Δ were solubilized and GIT1 immunoprecipitates blotted as indicated (IB). **(D)** GIT1/GluN3A control mTORC1 translation. Left: At early postnatal stages, immature synapses express GluN3A-NMDARs, which bind the postsynaptic scaffold GIT1 via their C-terminal tail preventing the nucleation of GIT1/mTORC1 and the mTORC1-mediated synthesis of plasticity proteins. Right: At juvenile/adult stages, GluN3A

down-regulation enables GIT1/mTOR/Raptor complex assembly and primes synapses for mTORC1-translation of mRNAs involved in synapse and memory consolidation. The genetic manipulations shown here to alter the timing of the age-dependent switch from mTOR-independent to mTOR-dependent modes of translation are indicated. Note that GluN3A expression is retained by subsets of synapses in adult brains and might play roles in selecting synapses that will be recruited to stably encode memory traces (see Discussion)**.** **(E)** Cortical neurons were infected with lentiviruses expressing GFP or GFP-sh3A on DIV3 and protein synthesis analyzed at DIV7-9. Representative blots and quantification of puromycin incorporation in infected neurons treated with rapamycin (100 nM), cycloheximide (CHX, 25 µM) or vehicle. **(F)** *Grin3a-/-* cortical neurons were infected with GFP, GFP-GluN3A or GFP-GluN3A1082Δ lentiviruses, and protein synthesis analyzed at DIV12. GluN3A expression and mTOR activation were monitored with the indicated antibodies (IB). In panels D-E, n= 4-7 from 3-4 independent cultures (*p<0.05, **p<0.01, ***p<0.001, two-way ANOVA followed by Tukey's test).

Figure 5 – figure supplement 1. Postnatal regulation of GIT1/mTOR complexes in mouse somatosensory cortex

Figure 5 – figure supplement 2. Age-dependent emergence of mTORC1-dependent protein synthesis in cortical neurons

Long-term memory formation is enhanced in *Grin3a*-deficient mice in a rapamycin-dependent manner

While GluN3A expression is typical of immature synapses at early postnatal stages as illustrated in our model, electron microscopy analyses demonstrate that subsets of synapses continue to express GluN3A into adulthood in areas such as the hippocampal CA1 (Roberts et al., 2009) and a recent mRNA expression study revealed that significant GluN3A levels are retained in a variety of brain regions (Murillo et al., 2021). Previous work showed that transgenic GluN3A overexpression impairs memory consolidation in hippocampal-dependent paradigms such as the Morris water maze (Roberts et al., 2009), but whether endogenous GluN3A expression has a physiological role in memory formation is unknown. We hypothesized that GluN3A modulation of synaptic mTORC1 signaling might provide a mechanism to set modes of translational control participating in memory encoding.

We reasoned that, if so, GluN3A deletion would create a permissive environment for stable memory formation and tested this by assessing mice learning in increasingly demanding tasks. Testing of *Grin3a*-/- mice in a standard version of the Morris water maze (4 trials per day) did not reveal differences in the latencies to reach the hidden platform relative to wild-type controls (Figure 6 - figure supplement 1A). Wild-type and *Grin3a*-/- mice displayed similar preferences for the target quadrant in probe trials where the platform was removed from the pool at the end of training, confirming that both had learnt the platform location (PT1; Figure 6 - figure supplement 1C). Differences emerged with a more demanding version of the task (2 trials per day): *Grin3a*-/- mice reached the platform significantly faster than wild-types, with shorter latencies by day 3 of training and greater preference for the target quadrant in probe trials (PT1; Figure 6A, B; Figure 6 - figure supplement 1B, D). No differences were observed in a visible version of the maze or in swim

velocities, suggesting that motor or perceptual differences do not account for the phenotype (Figure 6 - figure supplement 1E, F).

Similarly reduced learning thresholds had been reported in mice with elevated activity of mTOR or other pathways controlling translation (Banko et al., 2007; Costa-Mattioli et al., 2007; Hoeffer et al., 2008; Stern et al., 2013), often at the expense of impaired ability to respond to changed environments, altered memory fidelity, or appearance of perseverant and repetitive behaviors (Banko et al., 2007; Hoeffer et al., 2008; Santini et al., 2013 ; Shrestha et al., 2020b; Trinh et al., 2012). Thus we evaluated cognitive flexibility by re-training the mice to learn a new platform location ("reversal"). *Grin3a-/-* mice were better at shifting their preference relative to wild-type controls as evident in probe trials conducted 7 days after reversal (PT2; Figure 6A, B, Figure 6 - figure supplement 1B, D). No perseverative behavior was observed either in a Y-maze spontaneous alternation task (Figure 6 - figure supplement 1G). These results showed that GluN3A deletion facilitates spatial learning and memory without the unwanted effects associated to other modulators of translation.

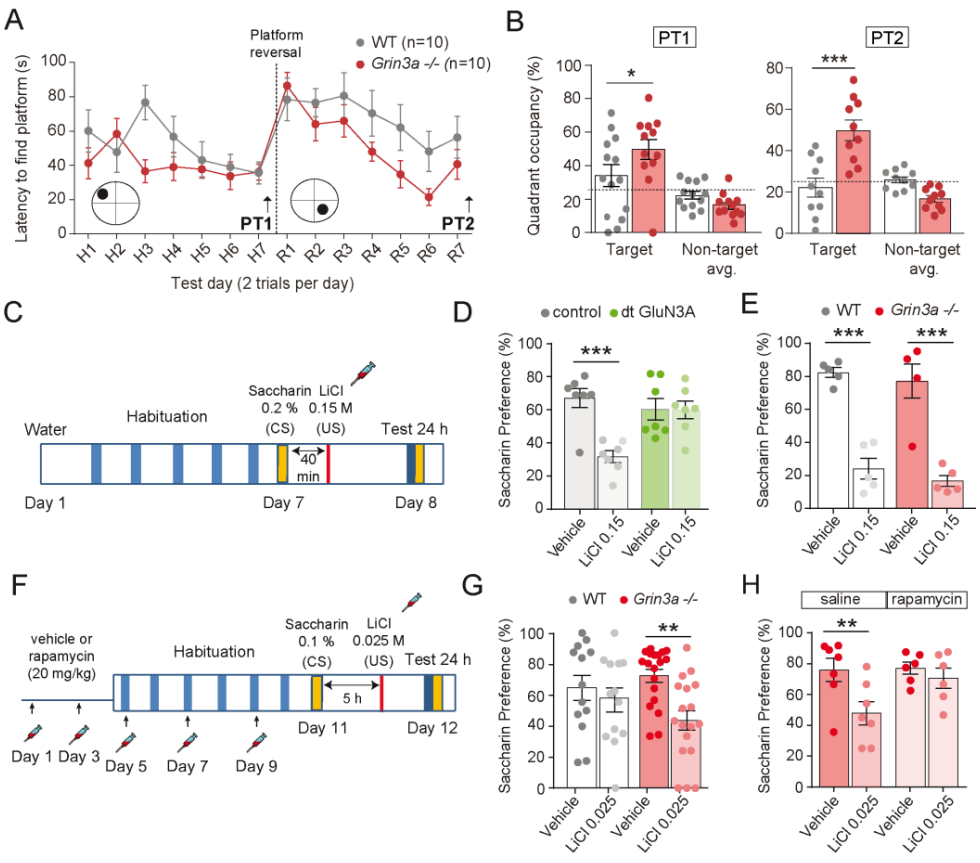

Figure 6. GluN3A deletion facilitates learning in spatial and associative tasks

(A) Escape latencies of male wild-type (WT) and *Grin3a-/-* mice on a weak version of the Morris water maze (2 trials/day) during 7-day training and after platform reversal on day 8. **(B)** Probe trials performed 24 hours after day 7 (PT1), or 24 hours after reversal training (PT2) (n=10-13 mice per genotype; two-way ANOVA with Bonferroni *post-hoc* test, *p<0.05, ***p<0.0001). **(C)** Conditioned taste aversion (CTA) paradigm. **(D)** Saccharin preference of control and double transgenic (dt) GluN3A mice, and **(E)** WT and *Grin3a-/-* mice after vehicle or LiCl injection (n=5-7 mice per group; ***p<0.001, two-way ANOVA followed by Bonferroni *post-hoc* test). **(F-H)** Weak CTA paradigm and rapamycin treatment regime. Decreased saccharin preference of *Grin3a-/-* mice on the weak CTA **(G)** was reversed by rapamycin **(H)** (**p<0.01, two-way ANOVA followed by Bonferroni *post-hoc* test).

Figure 6 – figure supplement 1. Behavior of male and female *Grin3a-/-* mice in the Morris Water Maze

Figure 6 – figure supplement 2. Controls for conditioned taste aversion (CTA) experiments

We then assessed long-term memory formation. For this we used two associative tasks that depend on new protein synthesis and can be achieved with the single pairing of a conditioned (CS) and unconditioned stimulus (US): conditioned taste aversion (CTA) and contextual fear conditioning. In CTA, a novel taste (saccharin, CS) is associated with an aversive US (LiCl, which induces nausea). The LiCl dose (US) and temporal contiguity between CS-US can be regulated to evaluate standard memory (Figure 6C), or "enhanced" memory by using a weaker paradigm (Figure 6F) (Adaikkan and Rosenblum, 2015). Transgenic mice with prolonged GluN3A expression into adulthood (dt GluN3A) displayed deficits in a standard CTA paradigm (US, LiCl 0.15 M i.p.) as judged by their similar preference for saccharin 24 hours after saline or LiCl injections (Figure 6D, green bars). This result was in-line with the memory deficits reported in other behavioral paradigms (Roberts et al., 2009). Control experiments ruled out the possibility that the defect was due to insensitivity to LiCl or to defects in distinguishing flavors (Figure 6 - figure supplement 2). By contrast, *Grin3a-/-* mice did not show differences relative to wild-types in a standard paradigm of CTA memory (Figure 6E). We then used a weak CTA paradigm where the strength of the US was reduced (LiCl 0.025 M), and US-CS were separated by 5 hours (Figure 6F). Under these conditions, only *Grin3a-/-* mice formed an association between CS-US, as shown by their significantly reduced preference for saccharin after LiCl injection but intact preference in wild-type controls. The negative association was long-lasting as it could be observed 24 (Figure 6G) and 48 hours after conditioning. To determine whether it was mTOR-dependent, we treated mice with a subthreshold dosing regime of rapamycin (Stoica et al., 2011) that does not affect standard CTA memory (Figure 6 - figure supplement 2). Rapamycin erased the weak CTA memory in *Grin3a-/-* mice (Figure 6H), supporting the notion that disinhibited mTOR signaling causes the cognitive enhancement.

In contextual fear conditioning, a particular environment (CS) is associated with a foot-shock (US) (Figure 7A). Wild-type and *Grin3a-/-* littermates showed similar freezing responses before the delivery of the foot-shock (Figure 7B). However, freezing was significantly stronger in *Grin3a-/-* mice 24 and 48 hours after a weak training protocol (single pairing of a tone with a 0.3 mA foot-shock, Figure 7B, C), demonstrating enhanced and lasting memory formation. No differences were observed in short-term (1 hour) memory that is protein-synthesis independent (Figure 7B). As in CTA, rapamycin occluded the difference between wild-type and *Grin3a-/-* mice (Figure 7C). Taken together, our behavioral results demonstrate that GluN3A deletion lowers the threshold for stable memory storage and provide pharmacological evidence linking the enhanced learning to a relief of GluN3A constraints on mTORC1 signaling.

Yet the cognitive enhancement could have been due to lack of GluN3A during development rather than adult stages. Also, GluN3A is expressed by excitatory neurons and somatostatin

interneurons, both recently implicated in protein-synthesis dependent memory consolidation (Sharma et al., 2020; Shrestha et al., 2020a). We therefore selectively ablated *Grin3a* from excitatory neurons or somatostatin-expressing interneurons by crossing floxed *Grin3a* mice (*Grin3a*$^{f/f}$) with mice that express Cre recombinase under the control of the Ca^{2+} calmodulin kinase IIα (*Camk2a*-Cre^{ERT2}) or somatostatin (*Sst*-Cre) promoter. The first strategy allowed conditional deletion of GluN3A at adult stages by injecting tamoxifen (Figure 7D). Biochemical analysis of adult hippocampal lysates confirmed effective deletion of GluN3A, and revealed that ~70% and ~20% of GluN3A protein is expressed by excitatory and somatostatin interneurons respectively (Figure 7 - figure supplement 1). We then subjected the mice to the weak fear conditioning protocol. Adult deletion of GluN3A from excitatory neurons was sufficient to enhance long-term memory, as shown by stronger freezing of *Grin3a*$^{f/f}$ x *Camk2a*-Cre^{ERT2} mice 24, 48 hours and even 7 days after training (Figure 7D). In contrast, *Grin3a*$^{f/f}$ x *Sst*-Cre and control mice exhibited similar freezing levels 24 and 48 hours after training (Figure 7E). Thus, adult GluN3A expression in excitatory neurons gates long-term memory formation.

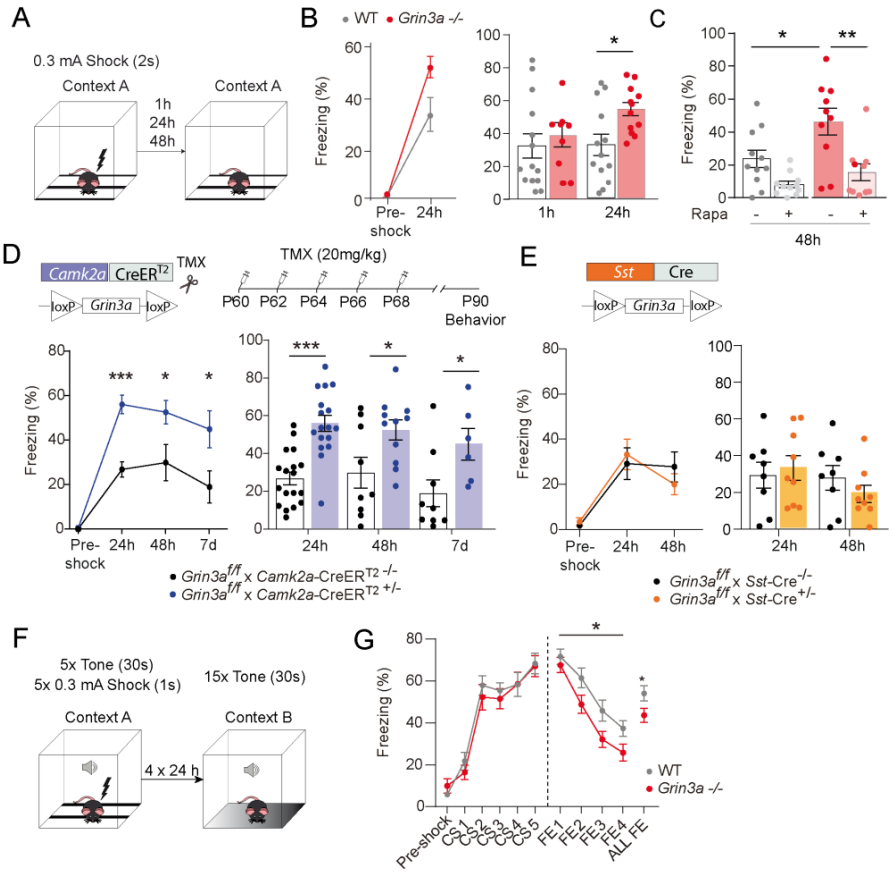

Figure 7. GluN3A deletion from excitatory neurons in adult mice is sufficient for memory enhancement

(A) Contextual fear conditioning test. (**B**) Enhanced contextual fear conditioning in *Grin3a-/-* mice 24 hours but not 1 hour after training (n=9-13 mice per group; left: repeated measures two-way ANOVA with Bonferroni *post-hoc* test, p=0.004; right: two-tailed unpaired t-test, *p<0.05). (**C**) *E*nhanced contextual fear conditioning in *Grin3a-/-* mice at 48 hours is reversed by rapamycin (n=10-11 mice per group; * p<0.05; ** p<0.01, two-way ANOVA with Bonferroni *post-hoc* test). **(D, E)** Conditional deletion of GluN3A from adult excitatory neurons, but not somatostatin (*Sst*) interneurons, enhances long-term contextual fear memory. The regime for tamoxifen (TMX) injection is indicated (*p<0.05: ***p<0.001 two-tailed unpaired t-test). **(F, G)** Cued-fear extinction in *Grin3a-/-* and wild-type littermates over a four-day fear extinction paradigm (n=14-13 mice per group; *p= 0.0461 between- subjects effect, repeated measures ANOVA).

Figure 7 – figure supplement 1. Expression of GluN3A and other synaptic proteins in conditional *Grin3a* knockout mice

Finally, we evaluated fear extinction, a form of memory where repeated presentation of a CS without reinforcement leads to the extinction of the acquired fear memory (Andero and Ressler, 2012). Fear extinction requires protein synthesis and is another indicator of behavioral flexibility that has been shown to be impaired after manipulation of general elements of translation. Mice were subjected to a strong auditory cued-fear conditioning protocol (5 pairings of a tone (CS) with a 0.3 mA foot-shock) followed by four cued-fear extinction sessions (15 CS alone, no foot-shock) (Figure 7F). Fear memory acquisition was similar between WT and *Grin3a*-/- littermates but fear extinction was enhanced in *Grin3a*-/- mice (Figure 7G), demonstrating that GluN3A deletion does not compromise the updating of memories but rather facilitates the extinction of fear memories.

DISCUSSION

In this study we report a regulatory mechanism that affords spatiotemporal control of mTORC1-dependent translation in response to synaptic stimulation. Specifically we identify GIT1/mTORC1 complexes as key mediators of synaptic mTORC1 responses, and demonstrate that GluN3A-NMDARs, through direct association with GIT1, impede GIT1/mTORC1 assembly and negatively regulate synaptic mTORC1 activation and mTORC1-dependent translation. Using *in vitro* and *in vivo* genetic approaches, we further show that negative regulation by GluN3A determines the emergence of mature mTORC1-dependent protein synthesis in developing brains, and continues to play a role in adult life by placing boundaries on long-term memory storage. More broadly, our findings suggest that neuronal GIT1/mTORC1 complexes might provide a central site for regulation and dysregulation of synaptic translation in other physiological and disease contexts.

Modulation by GluN3A of GIT1/mTORC1 complex assembly

mTORC1 is a ubiquitous protein kinase complex that promotes protein synthesis and cell growth in response to a variety of signals including nutrient availability, energy levels, insulin, growth factors and synaptic inputs. Coupling such diverse signals to mTORC1 activation requires the regulated targeting of mTOR to specific subcellular compartments. For instance, mTORC1 responses to amino acids require its recruitment by the Ragulator-Rag complex to lysosomal membranes, where interactions between positive (Rheb) and negative (Tsc1/2 complex) mTOR regulators take place (Benjamin and Hall, 2014; Sancak et al., 2010). Our observations suggest that GIT1 could play an analogous scaffolding role to position mTORC1 such that it senses synaptic signals, with negative regulation by GluN3A limiting mTORC1-dependent translation at specific developmental times or subsets of synapses in adult brains.

First, GIT1/mTORC1 complexes are located at dendritic/synaptic sites and respond to synaptic stimuli, as shown by phosphorylation of GIT1-bound mTOR on Ser^{2448}, an event downstream of the mTORC1 substrate S6K (Chiang and Abraham, 2005). Second, knocking-down GIT1 blunts synaptic mTORC1 signaling and mTORC1-dependent translation of specific activity-regulated genes. Third, GIT1/mTORC1 abundance increases during postnatal development and is bi-directionally modulated by GluN3A expression. A GluN3A mutant lacking the GIT1-binding site does not alter GIT1/mTORC1 assembly (Figure 5) or synaptic mTORC1 activation (Figure 3), demonstrating that association with GIT1 is required. Given that GluN3A and mTOR bind overlapping regions in GIT1 (Fiuza et al., 2013; Smithson and Gutmann, 2016), the most parsimonious explanation is that GluN3A competes with mTOR for binding to GIT1.

We previously reported that GluN3A modulates the formation of GIT1 complexes with βPIX (Fiuza et al., 2013), and might coordinately inhibit two central pathways for spine and memory consolidation —actin cytoskeletal rearrangements and protein synthesis— in a manner analogous to the translational repression by FMRP/CYFIP1 complexes (De Rubeis et al., 2013). Our results

here (see Figure 5B) indicate that GluN3A exerts a more potent regulation over GIT1/mTORC1 than GIT1/βPIX complexes and suggest that mTOR modulation might be the primary event. Of note, rare coding variants in GIT1 have been identified in schizophrenic patients (Kim et al., 2017) and GIT1 knockout mice display deficits that resemble those seen in mice with elevated GluN3A expression, including reduced spine size and poor learning and memory (Martyn et al., 2018). Additional phenotypes reported in mice and flies upon GIT1 deletion, such as microcephaly, reduced neuronal size or hyperactivity, might also be related to mTOR modulation (Hong and Mah, 2015; Won et al., 2011).

Our RNAseq analyses indicate that GluN3A acts at the level of translation and would thus preserve the supply of activity-induced plasticity mRNAs but restrict their active translation to specific synapses, in contrast to classical NMDARs that work at both transcriptional and translational levels. Nevertheless, GluN3A knockdown in cultured neurons has recently been shown to enhance the transcription of a subset of mRNAs (Chen et al., 2020) upon prolonged periods of synaptic activation (6-8 hours *vs* 1 hour in the present study), and we cannot rule out later regulation by GluN3A of compensatory or homeostatic responses. Of note, tonic repression of mTOR-dependent protein synthesis by GluN2B-containing NMDARs has also been reported (Wang et al., 2011). However, the molecular determinants of stimulation or repression of protein synthesis were not addressed and whether GluN3A and GluN2B share common mechanisms remains to be established.

A role for GluN3A in restricting translation for precise circuit refinements and long-term memory storage

GluN3A-NMDARs are highly expressed during critical periods of experience-dependent neural circuit refinements, when they have been proposed to determine which synapses will be maintained or eliminated, and at lower levels in specific regions of the adult brain (Murillo et al., 2021). We propose a model whereby the lack or presence of GluN3A at postsynaptic sites contributes to spine-specific translation by setting a GO or NO-GO biochemical environment for mTORC1 signaling that will depend on the stage of brain development (Figure 5D) but also on the activity history of individual synapses, which is a key aspect in theories of cellular consolidation (Redondo and Morris, 2011). That is: synaptic GluN3A levels are down-regulated by sensory experience and can be controlled at the level of individual synapses by activity-dependent endocytosis (Perez-Otano et al., 2006). Removal of GluN3A-NMDARs from active synapses would drive GIT1/mTORC1 complex formation, creating the potential for translation of activity-regulated mRNAs and giving active inputs an advantage for consolidation *vs* less-active neighbors. Hence, competition for mTORC1 signaling machinery would provide the means for selective synapse stabilization and storage of relevant events (see below), while defects in this process would permit the consolidation of otherwise lost synaptic changes. Such competition-based model is supported by observations such as the

localization of GluN3A to subsets of adult synapses (Roberts et al., 2009) or the enhanced GIT1/mTORC1 availability and capacity for memory storage of *Grin3a-/-* mice, which becomes apparent with light training protocols normally insufficient for attaining stable memories in wild-type mice and which can be reversed by rapamycin. Importantly, several models postulate that the restriction of protein synthesis to sites of active translation underlies phenomena such as the competition between spines for lasting LTP expression or the clustered dendritic plasticity (Fonseca et al., 2004; Govindarajan et al., 2011). Incorporation into these models of the molecular components unveiled here might open avenues for testing how these phenomena determine memory capacity and efficiency and for correcting cognitive dysfunction.

Our experiments using cell-type specific and inducible *Grin3a* knockout mice demonstrate a role of GluN3A in gating cognitive processing in the adult brain beyond its better recognized functions in postnatal neural circuit refinements, and identify excitatory neurons as the locus of GluN3A actions. In relation to memory, negative regulators are thought to provide an advantage by ensuring that only salient features are learnt and filtering out irrelevant events or associations (Abel et al., 1998; Cho et al., 2015). For instance, temporal contiguity of events is required for many forms of associative learning; within the scale of seconds or minutes for classical conditioning paradigms, longer in other types of memory. In CTA the CS and US can be hours apart, with temporal boundaries set by the strength of the US (Adaikkan and Rosenblum, 2015). Our results show that the absence of GluN3A broadens this temporal limit and facilitates learning of demanding tasks, i.e. where training is spaced apart or the presented stimuli are weaker. The reversal by rapamycin strongly suggests that the enhanced readiness of the mTORC1 translational machinery in GluN3A-deficient mice expands the range for consolidation of memory traces. As far as tested here, GluN3A deletion does not impair other aspects of cognition such as memory flexibility or extinction. Yet significant GluN3A levels are retained in defined areas of the mouse and human adult brain that have in common strong plasticity or functional integration needs (Fulcher et al., 2019; Murillo et al., 2021), and a recent study linked adult GluN3A expression to the control of emotional states (Otsu et al., 2019). In addition, genetic variations in *GRIN3A* have been shown to modulate prefrontal cortex activity (Gallinat et al., 2007) and episodic memory (Papenberg et al., 2014). Future investigations should determine whether domains of cognition other than the ones we tested are compromised by GluN3A deletion.

GluN3A and synaptic protein translation as selective therapeutic targets

The stabilization of memories requires de novo protein expression. Nevertheless, the effects on cognition of enhancing mTOR signaling or protein synthesis are perplexing. Loss of constraints on protein synthesis due to mutations in negative regulators of translation (*FMR1*, *MECP2*, or mTORC1 suppressors including *NF1*, *TSC1/2* or the phosphatase *PTEN)* are associated with cognitive impairment and high incidence of autism spectrum disorders and intellectual disability (Kelleher and

Bear, 2008), although a fraction of autistic individuals exhibit enhanced cognitive skills within specific domains (Heaton and Wallace, 2004). On the other hand, inhibiting the phosphorylation of eIF2α, which generally increases translation (Costa-Mattioli et al., 2007; Stern et al., 2013), or enhancing mTORC1 activity by removal of FKBP12 (Hoeffer et al., 2008) have been reported to lower memory thresholds. However, the cognitive enhancement came at the cost of reduced memory fidelity and cognitive flexibility even when cell-type specific modulation was attempted (Santini et al., 2013; Shrestha et al., 2020a; Trinh et al., 2012), which we did not observe here. Key differences could be that negative regulators of mTOR such as FMRP, PTEN or Tsc1/2 lack neuronal/synapse specificity, as demonstrated by their linkage to altered cell growth and appearance of tumors (Lipton and Sahin, 2014). Also, in some of the above situations, translation is constitutively activated and responses to incoming signals might be obliterated. By contrast, lack of GluN3A does not occlude mTORC1 activation but rather seems to prime mTOR activation by synaptic stimuli. At present, the enhancement of learning and memory produced by loss of GluN3A suggests that targeting GluN3A expression or signaling functions might be of therapeutic benefit. For instance, small molecules that perturb the GluN3A/GIT1 association might work in subtler ways than general translation regulators by specifically modulating synaptic mTORC1 signaling.

AUTHOR CONTRIBUTIONS

P.N.D., M.J.C.D., and I.P.O. designed the study, performed and analyzed the molecular and biochemical experiments, prepared and wrote the manuscript. O.E.Z. and L.G.R. designed, performed and analyzed the behavioral experiments. R.A. and E.R.V. conducted the fear extinction task. J.F.W., C. G. L., F.G. and V.B. designed and assisted with molecular biology and biochemical experiments. S.N. and A.B. performed bioinformatic analysis of RNAseq data. S.J.T., T.G. and P.P. performed and analyzed the electrophysiological experiments.

ACKNOWLEDGEMENTS

We thank Stuart Lipton and Nobuki Nakanishi for providing the *Grin3a* knockout mice, Beverly Davidson for the AAV-caRheb, Jose Esteban for help with behavioral and biochemical experiments, and Noelia Campillo, Rebeca Martínez-Turrillas and Ana Navarro for expert technical help. Work was funded by the UTE project CIMA; fellowships from the Fundación Tatiana Pérez de Guzmán el Bueno, FEBS and IBRO (to M.J.C.D.), Generalitat Valenciana (to O.E-Z.), Juan de la Cierva (to L.G.R), FPI-MINECO (to E.R.V., to S.N.) and Intertalentum postdoctoral program (to V.B.); ANR (GluBrain3A) and ERC Advanced Grants (#693021) (to P.P.); Ramón y Cajal program RYC2014-15784, RETOS-MINECO SAF2016-76565-R, ERANET-Neuron JTC 2019 ISCIII AC19/00077 FEDER funds (to R.A.); RETOS-MINECO SAF2017-87928-R (to A.B.); an NIH grant (NS76637) and UTHSC College of Medicine funds (to S.J.T); and NARSAD Independent Investigator Award and

grants from the MINECO (CSD2008-00005, SAF2013-48983R, SAF2016-80895-R), Generalitat Valenciana (PROMETEO 2019/020)(to I.P.O) and Severo-Ochoa Excellence Awards (SEV-2013-0317, SEV-2017-0723).

DECLARATION OF INTERESTS

The authors declare no competing financial interests

MATERIAL AND METHODS

Animals

Adult (3-6 months old) *Grin3a*-/-, *Grin3a*$^{tm1a(EUCOMM)Hmgu}$/H (*Grin3a*$^{f/f}$) and double-transgenic GFP-GluN3A (dtGluN3A) mice backcrossed for 10-12 generations into a C57Bl6/J background were used. Single transgenic mice were used as controls for dtGluN3A mice, and wild-type littermates from heterozygote crosses were controls for *Grin3a-/-* mice. Commercial C57BL6/J mice were purchased from Charles River Laboratories. For time-specific knockout of *Grin3a* in excitatory neurons, tamoxifen-inducible CaMKIIα-CreERT2$^{+/-}$ mice (Erdmann et al., 2007) were crossed with *Grin3a*$^{f/f}$ mice. Tamoxifen (Sigma-Aldrich T5648, 20 mg/ml dissolved in corn oil) was administered via oral gavage (5 alternate days). For inhibitory neuron-specific knockout of *Grin3a*, Sst-IRES-Cre$^{+/-}$ mice (JAX Stock No. 018973) were backcrossed with C57BL/6J mice for 12 generations and then bred with *Grin3a*$^{f/f}$ mice. Male mice were used for behavioral experiments unless indicated. Animals were housed four to six per cage with *ad libitum* access to food and water and maintained in a temperature-controlled environment on a 12 h dark/light cycle. All procedures were conducted in accordance with the European and Spanish regulations (2010/63/UE; RD 53/2013) and were approved by the Ethical Committee of the Generalitat Valenciana (2017/VSC/PEA/00196). For the cued-fear conditioning experiments, ethic protocols were approved by the Committee of Ethics of the Universitat Autònoma de Barcelona and the Generalitat de Catalunya.

Primary neuronal cultures

Cortical neurons in primary culture were prepared as described (Perez-Otano et al., 2006). Briefly, cortices were dissected from E19 rat pups or E17.5 mice pups and dissociated with papain (Worthington Biochemical). Neurons were plated at 75,000 cells per well on 12-wells plates, 500,000 cells per well on 6-wells plates and 1,000,000 cells/ dish on 60mm dishes coated with laminin and poly-D-lysine and grown in Neurobasal Medium supplemented with B27 (ThermoFisher).

Neurons were infected with lentiviruses 5 days prior to collection (timing of infection is indicated in figure legends). Neurotrophic factors and other drugs were used at the following concentrations: anisomycin (0.8 μM, Sigma-Aldrich A5892), recombinant human BDNF (100 ng/ml, PeproTech 450-02), bicuculline (50 μM, Abcam Ab120108), cycloheximide (25 μM, Sigma Aldrich C7698), (D,L)-APV (50 μM, Tocris 3693), MK801 (10 μM, Tocris 0924), rapamycin (100 nM, Alfa Aesar J62473) and puromycin (10 ng/ml, Sigma Aldrich P8833).

Lentiviral vectors

For the generation of lentiviral constructs, full-length GluN3A and GluN3A1082Δ cDNAs were subcloned into a dual lentiviral vector Syn-WPRE-Syn-GFP kindly provided by Dr. Francisco G Scholl, University of Sevilla, Spain. For knockdown experiments, 19-20 base pairs (bp)-long small

hairpin RNAs (shRNA) directed to GluN3A (shGluN3A1185, target sequence: CTACAGCTGAGTTTAGAAA) or GIT1 (shGIT1, target sequence: TGATCACAAGAATGGGCATTA) were cloned into the pLentilox 3.7-GFP vector downstream the U6 promoter. The AAV encoding constitutively active human Rheb (AAV-caRheb, S16H) was kindly provided by Dr. Beverly Davidson, Children´s Hospital of Philadelphia, University of Pennsylvania.

RNA isolation, qRT-PCR and RNAseq analyses

Total RNA from cultured cortical neurons was isolated using the Nucleospin RNA (Macherey-Nagel). RNA concentration and purity were assessed with NanoDrop™. RNA quality was determined by the RNA Integrity Number (RIN) algorithm using the Agilent® 2100 Bionalyzer Instrument; only samples with RIN>9 matched our standard.

For qRT-PCR experiments, first-strand cDNA was synthesized from 1 µg of total RNA using the Invitrogen SuperScript IV First-Strand cDNA Synthesis System (ThermoFisher). Quantitative real-time PCR (qPCR) was performed using the Applied Biosystems QuantStudio 3 Real-Time PCR system and analyzed with the QuantStudio 3 Design and Analysis software (v1.5.1,ThermoFisher). Briefly, real-time qPCR was assayed in a total volume of 20 µl reaction mixture containing the ready-to-use PyroTaq EvaGreen qPCR Mix Plus ROX (Cmb), 5pmol of forward and reverse (rv) primers (detailed in Table S1) and cDNA. PCR thermal conditions included an initial hold stage with 5 min at 50ºC and 15 min at 95 °C followed by 40 cycles of denaturation for 30 s at 95 °C, annealing for 32 s at 60 ºC and primer elongation for 32 s at 72 °C. All qPCR reactions were run in triplicates. Mean cycle threshold (Ct) values for each reaction were recorded and the relative RNA expression levels were calculated referring to *Gapdh,* encoding glyceraldehyde 3-phsophate dehydrogenase: $\Delta Ct = \llbracket Ct \rrbracket\_GAPDH - \llbracket Ct \rrbracket\_(target\ gene)$. The gene expression fold change normalized to GAPDH and relative to control sample was calculated as 2^ΔCt.

For RNAseq experiments, we performed bulk mRNA sequencing single-end with a length of 50bp using the RNAseq Illumina Hiseq2500. The preparation of the polyA sequencing library, library's quality control and quantification, sequencing run and base calling data were carried out by the Genomics Core Facility of the Centre for Genomic Regulation (CRG, Barcelona). For the analysis, adapters were trimmed using trim_galore v0.6.4_dev and reads with longer length than 40 bp were selected. Trimmed reads were aligned using star c2.6.1b to the mouse genome (mm10). Reads with mapq >30 were selected using Samtools v1.9. Mapped reads were quantified using R scripts (R version 4.0.3, 2020), Rsubread v2.4.3 and the Mus_musculus.GRCm38.99.gtf annotation data. Differential expression analysis was performed using DESeq2 1.31.1 and limma 3.46.0; genes were annotated using biomaRt v2.46.3 and Volcano plots were performed with EnhancedVolcano 1.6.0. The tracks from the samples were performed with DeepTools v3.5.0, normalized with RPKM and visualization was done in IGV v2.6.3.

Protein extraction and western blotting

Cultured neurons were collected in lysis buffer containing 50 mM Tris-HCl pH 6.8, 10% glycerol, 2% SDS, 0.1 M (D,L)-Dithiothreitol, 0.04% bromophenol blue and supplemented with protease (cOmplete Protease Inhibitor Cocktail) and phosphatase (PhosSTOP) inhibitors. Lysates were incubated for 10 min at 65 ºC, briefly centrifuged at maximum speed, separated by SDS-PAGE and immunoblotted as described (Fiuza et al., 2013) using the antibodies indicated in the Table S2. Specific bands were quantified using the ImageQuant 5.2 software.

For *in vivo* studies on mouse tissue, hippocampi and somatosensory cortex were dissected on ice, snapped frozen in liquid nitrogen and stored at -80ºC until processing. Tissues were homogenized in 15 (w/v) volumes of modified ice-cold RIPA buffer (50 mM Tris-HCl pH 7.5, 150 mM NaCl, 1% NP-40, 0.05% deoxycholate, 0.01% SDS) supplemented with protease and phosphatase inhibitors, sonicated and centrifuged for 20 min at 16,200 x g at 4ºC. Protein content was estimated using a Pierce BCA Assay kit (ThermoFisher) before immunoblotting.

Immunoprecipitation

Cultured cortical neurons or mouse hippocampus or somatosensory cortex were solubilized for 30 min in cold lysis buffer containing 0.1% Triton X-100, 0.1% SDS, 150 mM NaCl, 10 mM EDTA and 50 mM HEPES or 0.3% CHAPS, 150 mM NaCl, 1 mM EDTA and 40 mM HEPES, supplemented with protease and phosphatase inhibitors. Insoluble material was removed by centrifugation at 16,200 x g for 15 min and 100-150 μg of the resulting supernatants were incubated overnight at 4 °C with or without (IgG-) the immunoprecipitating antibody. Lysates were then incubated with protein A/ G magnetic beads (BioRad) for 2 h at 4 ºC. Beads were precipitated using a magnetic rack, washed thrice in lysis buffer and immunoprecipitated proteins were eluted with SDS sample buffer and analyzed by western blotting.

Proximity Ligation Assay

Cultured neurons transfected with pRK5-GFP were fixed at DIV17 with 4% PFA, 4% sucrose in PBS (RT, 10 min), incubated with blocking solution and permeabilized. Cells were then incubated with rabbit polyclonal anti-mTOR antibody and mouse monoclonal anti-GIT1 antibody overnight at 4°C, washed with PBS, and incubated for 1 h with PLA secondary probes (anti-mouse Plus and anti-rabbit Minus, Olink Bioscience) at 37 °C. Cells were washed twice with Duolink II Wash Buffer A (Olink Bioscience) and incubated with the ligase (1:40; Olink Bioscience) in ligase buffer for 30 min at 37 °C. After additional washes with Buffer A, cells were incubated with DNA polymerase (1:80; Olink Bioscience) in amplification buffer for 100 min at 37 °C in the dark. Cells were then washed with Duolink II Wash Buffer B (Olink Bioscience) and incubated with chicken polyclonal anti-GFP for 1 h at room temperature. After washing with PBS, cells were incubated with secondary goat anti-chicken-Alexa Fluor 488 for 1 h at room temperature. Finally, cells were washed in PBS and mounted on slides with Fluoroshield mounting medium (Sigma-Aldrich). Fluorescence images were

acquired by using Nikon A1 Ti2 system with a sequential acquisition setting at 1024 x 1024 pixels resolution; cells were randomly selected from different coverslips.

Protein synthesis assays

Basal protein translation was measured using a SUnSET (surface sensing of translation) assay. Briefly, primary cortical cultures were treated with 10 ng/ ml of puromycin for 30 min and lysed as described above. Untreated neurons and neurons preincubated with the protein synthesis inhibitor cycloheximide (15 min before puromycin) were used as controls. Proteins were resolved by SDS-PAGE and analyzed by western blotting using an anti-puromycin antibody. Ponceau S staining was used as protein loading control.

Behavioral analysis

Morris Water Maze: Mice were trained to find a submerged platform in a circular tank (190 cm diameter) filled with opaque white water in two or four trials per day with 45 min inter-trial intervals. If mice did not find the platform in 120 seconds, they were kindly guided to it. The hidden platform was relocated to the opposite quadrant after 7 days of training for the reversal training phase. 60-second-long probe tests in which platform was removed were performed at the end of each phase (PT1, after initial hidden platform learning; PT2, after reversal learning), and time spent in the target quadrant was compared to the average time spent in all other quadrants. Mice were tracked throughout the whole protocol using the video-tracking software SMART (Panlab S. L.).

Y-maze spontaneous alternation: Mice were introduced in a three-armed Y-shaped maze and recorded for 5 minutes. Correct triad scores were noted when all three arms were sequentially entered. Alternation indices were calculated as correct triads / possible triads. Maze was cleaned between animals with a water-based soap solution.

Conditioned Taste Aversion: Test was adapted from (Adaikkan and Rosenblum, 2015). In brief: mice were trained to drink from two bottles of water for 6 days. On conditioning day, water was changed for 0.2% (regular CTA) or 0.1% (weak CTA) saccharin for 40 minutes (regular) or 5 hours (weak) after the exposure, mice were injected LiCl intraperitoneally at 0.15 M (regular) or 0.025 M (weak). Saccharin preference was evaluated 24 hours after injection. For unconditioned taste preference, mice were presented two drinking bottles for 48 hours: one contained water and the other one of the following solutions: Sucrose 5% (sweet), NaCl 75 mM (salty), Quinine 300 µM (bitter) and HCl 0.03 M (sour). Bottle sides were switched after 24 hours to avoid potential side bias. Solution preference was evaluated at 48 hours. For assessing sensitivity to LiCl toxicity, “lying on belly” behavior was registered after injection of LiCl (0.15 M) or saline. This behavior consists in a totally general suppression of activity, and location of the mouse in the corner of a cage. The activity was measured for 20 minutes.

Fear conditioning and extinction: Fear conditioning (FC) and extinction (FE) procedures were carried out with a computerized Fear and Startle system (Panlab-Harvard, Barcelona, Spain). Tones

and shocks were delivered and controlled using Freezing v1.3.04 software (Panlab-Harvard, Barcelona, Spain). The fear chambers consisted of a black methacrylate box with a transparent front door (25x25x25cm) inside a sound-attenuating cubicle (67x53x55cm). Animals were habituated to the chambers for 5 min/day during two consecutive days prior to FC. The chambers were carefully cleaned before and after each mouse.

For contextual FC, mice were placed in the fear chambers and allowed to explore a context (CS) (metal grid floor, no light source) for 2 minutes. Mice were then presented with a tone (30s, 2.8 kHz, 85 dB tone) that co-terminated with a foot shock (US)(0.3 mA, 2s). Sixty seconds later, they were returned to their home cage. Conditioning was assessed at 1 (short-term memory), 24 and 48 hours or 7 days (long-term memory) by re-introducing mice in the conditioning context for 5 minutes. Freezing behavior, a rodent´s natural response to fear defined as the absence of movement except respiration, was scored by a high sensitivity weight transducer system located at the bottom of the experimental chambers which records and analyses the signal generated by the movement of the animal.

For cued FC, mice were placed in the fear chambers for 5 minutes and then received 5 trials of a tone (CS) (30 s, 6 kHz, 75 dB) that co-terminated with a foot-shock (US) (0.3 mA, 1s). The intertrial interval (ITI) was of 3 minutes, and 3 additional minutes followed the last trial. The FE sessions were performed 4 times in consecutive days (FE1, FE2, FE3, FE4) starting 24h after FC. For FE, mice were placed in the fear chambers for 5 minutes and then exposed to 15 trials of the 30 s CS tone alone (cued-fear) with a 30 s of ITI interval. An additional 30 s interval followed the last trial of FE. Different contexts were used for FC and FE tests. FC context consisted of a yellow light source (~10 lux), a grid floor of 25 bars (3 mm Ø and 10 mm between bars), a background noise of 60 dB produced by a ventilation fan and soapy water in a solution of ethanol 70% was used for cleaning between sessions. FE context consisted of a red-light source (~10 lux), a grey plexiglass floor covering the bars, no background noise and soapy water in a solution of isopropyl alcohol 40% was used as cleaning agent between sessions. Different routes were used to transport animals from their home cages to testing room in FC and FE days. Freezing levels were scored and averaged in 30 second slots.

Electrophysiology

HEK293 cells were cultured, transfected, and recorded as previously described using GluN1A and GluN2A in pcDNA1/Amp and GFP-tagged GluN3A or GluN3A1082Δ subcloned in pCI-neo (Chowdhury et al., 2013). Briefly, cells were transfected with GluN1-1A, GluN2A, and either GFP-GluN3A or GFP-GluN3A1082Δ in a 1:1:3 ratio and maintained in medium with APV (250 μM). GFP was used as a transfection marker in cells where GluN3A constructs were omitted. Whole-cell recordings were made with on GFP-positive cells using a Multiclamp 700A amplifier (Molecular Devices) 24 h following transfection. Patch pipettes (2 to 4 MΩ) contained (in mM): 140 Cs

methanesulfonate, 10 HEPES, 5 adenosine triphosphate (Na salt), 5 $MgCl_2$, 0.2 $CaCl_2$, and 10 BAPTA (pH 7.4). The extracellular solution contained (in mM) 150 NaCl, 5 KCl, 2 or 10 $CaCl_2$, 10 HEPES, 10 glucose (pH 7.4) and was adjusted to 330 mOsm with sucrose. Currents were digitized at 2 kHz and filtered at 1 kHz. Series resistance (90 to 95%) and whole-cell capacitance compensation were employed. Experiments were performed at a holding potential of -80 mV with ramps (300 ms to +50 mV) elicited following a 3 s application of glutamate (1 mM) and glycine (100 μM) at 20°C. The ΔE_{rev}, was calculated by subtracting the E_{rev} obtained in 2 mM Ca^{2+} from the E_{rev} measured in 10 mM Ca^{2+} and corrected for the junction potential between solutions. Initial peak currents were obtained from 1 sec agonist applications in 2 mM Ca^{2+} and used to calculate the current density. Experiments on glycine-gated diheteromeric GluN1/GluN3A receptors expressed in HEK293 cells were performed as previously described (Grand et al., 2018) using GluN1-1a and GFP-GluN3A or GFP-GluN3A1082Δ subcloned in pCI-neo (see above).

Statistical Analysis

Statistical analyses were conducted with GraphPad Prism software. Comparison of quantitative variables between two groups was performed using Student's t-test. One-way or two-way analysis of variance (ANOVA) followed by a post-hoc comparison test were used when more than two groups were compared, as indicated in the corresponding figure legend. Results are presented as mean ± standard error of the mean (s.e.m.). Statistical methods used for behavioral studies are indicated in the corresponding figure legends.

Data availability

RNAseq data have been deposited at GEO-NCBI under the access code GSE175920. Raw Western blots for each figure are presented in source-data-files.

REFERENCES

Abel, T., Martin, K.C., Bartsch, D., and Kandel, E.R. (1998). Memory suppressor genes: inhibitory constraints on the storage of long-term memory. Science *279*, 338-341.

Adaikkan, C., and Rosenblum, K. (2015). A molecular mechanism underlying gustatory memory trace for an association in the insular cortex. Elife *4*, e07582.

Andero, R., and Ressler, K.J. (2012). Fear extinction and BDNF: translating animal models of PTSD to the clinic. Genes Brain Behav *11*, 503-512.

Banko, J.L., Merhav, M., Stern, E., Sonenberg, N., Rosenblum, K., and Klann, E. (2007). Behavioral alterations in mice lacking the translation repressor 4E-BP2. Neurobiol Learn Mem *87*, 248-256.

Benjamin, D., and Hall, M.N. (2014). mTORC1: turning off is just as important as turning on. Cell *156*, 627-628.

Cammalleri, M., Lutjens, R., Berton, F., King, A.R., Simpson, C., Francesconi, W., and Sanna, P.P. (2003). Time-restricted role for dendritic activation of the mTOR-p70S6K pathway in the induction of late-phase long-term potentiation in the CA1. Proc Natl Acad Sci U S A *100*, 14368-14373.

Costa-Mattioli, M., Gobert, D., Stern, E., Gamache, K., Colina, R., Cuello, C., Sossin, W., Kaufman, R., Pelletier, J., Rosenblum, K*., et al.* (2007). eIF2alpha phosphorylation bidirectionally regulates the switch from short- to long-term synaptic plasticity and memory. Cell *129*, 195-206.

Costa-Mattioli, M., and Monteggia, L.M. (2013). mTOR complexes in neurodevelopmental and neuropsychiatric disorders. Nat Neurosci *16*, 1537-1543.

Chen, L.F., Lyons, M.R., Liu, F., Green, M.V., Hedrick, N.G., Williams, A.B., Narayanan, A., Yasuda, R., and West, A.E. (2020). The NMDA receptor subunit GluN3A regulates synaptic activity-induced and myocyte enhancer factor 2C (MEF2C)-dependent transcription. J Biol Chem *295*, 8613-8627.

Chiang, G.G., and Abraham, R.T. (2005). Phosphorylation of mammalian target of rapamycin (mTOR) at Ser-2448 is mediated by p70S6 kinase. J Biol Chem *280*, 25485-25490.

Cho, J., Yu, N.K., Choi, J.H., Sim, S.E., Kang, S.J., Kwak, C., Lee, S.W., Kim, J.I., Choi, D.I., Kim, V.N*., et al.* (2015). Multiple repressive mechanisms in the hippocampus during memory formation. Science *350*, 82-87.

Chowdhury, D., Marco, S., Brooks, I.M., Zandueta, A., Rao, Y., Haucke, V., Wesseling, J.F., Tavalin, S.J., and Perez-Otano, I. (2013). Tyrosine phosphorylation regulates the endocytosis and surface expression of GluN3A-containing NMDA receptors. J Neurosci *33*, 4151-4164.

De Rubeis, S., Pasciuto, E., Li, K.W., Fernandez, E., Di Marino, D., Buzzi, A., Ostroff, L.E., Klann, E., Zwartkruis, F.J., Komiyama, N.H*., et al.* (2013). CYFIP1 coordinates mRNA translation and cytoskeleton remodeling to ensure proper dendritic spine formation. Neuron *79*, 1169-1182.

Erdmann, G., Schutz, G., and Berger, S. (2007). Inducible gene inactivation in neurons of the adult mouse forebrain. BMC Neurosci *8*, 63.

Fiuza, M., Gonzalez-Gonzalez, I., and Perez-Otano, I. (2013). GluN3A expression restricts spine maturation via inhibition of GIT1/Rac1 signaling. Proc Natl Acad Sci U S A *110*, 20807-20812.

Flavell, S.W., and Greenberg, M.E. (2008). Signaling mechanisms linking neuronal activity to gene expression and plasticity of the nervous system. Annual review of neuroscience *31*, 563-590.

Fonseca, R., Nagerl, U.V., Morris, R.G., and Bonhoeffer, T. (2004). Competing for memory: hippocampal LTP under regimes of reduced protein synthesis. Neuron *44*, 1011-1020.

Fulcher, B.D., Murray, J.D., Zerbi, V., and Wang, X.J. (2019). Multimodal gradients across mouse cortex. Proc Natl Acad Sci U S A *116*, 4689-4695.

Gallinat, J., Gotz, T., Kalus, P., Bajbouj, M., Sander, T., and Winterer, G. (2007). Genetic variations of the NR3A subunit of the NMDA receptor modulate prefrontal cerebral activity in humans. Journal of cognitive neuroscience *19*, 59-68.

Govindarajan, A., Israely, I., Huang, S.Y., and Tonegawa, S. (2011). The dendritic branch is the preferred integrative unit for protein synthesis-dependent LTP. Neuron *69*, 132-146.

Grand, T., Abi Gerges, S., David, M., Diana, M.A., and Paoletti, P. (2018). Unmasking GluN1/GluN3A excitatory glycine NMDA receptors. Nat Commun *9*, 4769.

Greenwood, T., LC, L., AX, M., NR, S., ME, C., R, F., MF, G., GA, L., CM, N., KH, N.*, et al.* (2019). Genome-wide Association of Endophenotypes for Schizophrenia From the Consortium on the Genetics of Schizophrenia (COGS) Study. JAMA Psychiatry *76*, 1274-1284.

Hardingham, G.E., Fukunaga, Y., and Bading, H. (2002). Extrasynaptic NMDARs oppose synaptic NMDARs by triggering CREB shut-off and cell death pathways. Nat Neurosci *5*, 405-414.

Heaton, P., and Wallace, G.L. (2004). Annotation: the savant syndrome. Journal of child psychology and psychiatry, and allied disciplines *45*, 899-911.

Henson, M.A., Larsen, R.S., Lawson, S.N., Perez-Otano, I., Nakanishi, N., Lipton, S.A., and Philpot, B.D. (2012). Genetic deletion of NR3A accelerates glutamatergic synapse maturation. PLoS One *7*, e42327.

Hoeffer, C.A., Tang, W., Wong, H., Santillan, A., Patterson, R.J., Martinez, L.A., Tejada-Simon, M.V., Paylor, R., Hamilton, S.L., and Klann, E. (2008). Removal of FKBP12 enhances mTOR-Raptor interactions, LTP, memory, and perseverative/repetitive behavior. Neuron *60*, 832-845.

Holt, C.E., Martin, K.C., and Schuman, E.M. (2019). Local translation in neurons: visualization and function. Nat Struct Mol Biol *26*, 557-566.

Holtmaat, A., and Caroni, P. (2016). Functional and structural underpinnings of neuronal assembly formation in learning. Nat Neurosci *19*, 1553-1562.

Hong, S.T., and Mah, W. (2015). A Critical Role of GIT1 in Vertebrate and Invertebrate Brain Development. Exp Neurobiol *24*, 8-16.

Hou, L., and Klann, E. (2004). Activation of the phosphoinositide 3-kinase-Akt-mammalian target of rapamycin signaling pathway is required for metabotropic glutamate receptor-dependent long-term depression. J Neurosci *24*, 6352-6361.

Huang, X., Chen, Y.Y., Shen, Y., Cao, X., Li, A., Liu, Q., Li, Z., Zhang, L.B., Dai, W., Tan, T.*, et al.* (2017). Methamphetamine abuse impairs motor cortical plasticity and function. Mol Psychiatry *22*, 1274-1281.

Josselyn, S.A., and Tonegawa, S. (2020). Memory engrams: Recalling the past and imagining the future. Science *367*.

Kehoe, L.A., Bellone, C., De Roo, M., Zandueta, A., Dey, P.N., Perez-Otano, I., and Muller, D. (2014). GluN3A promotes dendritic spine pruning and destabilization during postnatal development. J Neurosci *34*, 9213-9221.

Kelleher, R.J., 3rd, and Bear, M.F. (2008). The autistic neuron: troubled translation? Cell *135*, 401-406.

Kim, M.J., Biag, J., Fass, D.M., Lewis, M.C., Zhang, Q., Fleishman, M., Gangwar, S.P., Machius, M., Fromer, M., Purcell, S.M.*, et al.* (2017). Functional analysis of rare variants found in schizophrenia implicates a critical role for GIT1-PAK3 signaling in neuroplasticity. Mol Psychiatry *22*, 417-429.

Klann, E., and Dever, T.E. (2004). Biochemical mechanisms for translational regulation in synaptic plasticity. Nat Rev Neurosci *5*, 931-942.

Lipton, J.O., and Sahin, M. (2014). The neurology of mTOR. Neuron *84*, 275-291.

Liu, G.Y., and Sabatini, D.M. (2020). mTOR at the nexus of nutrition, growth, ageing and disease. Nat Rev Mol Cell Biol *21*, 183-203.

Lyons, M.R., and West, A.E. (2011). Mechanisms of specificity in neuronal activity-regulated gene transcription. Prog Neurobiol *94*, 259-295.

Marco, S., Giralt, A., Petrovic, M.M., Pouladi, M.A., Martinez-Turrillas, R., Martinez-Hernandez, J., Kaltenbach, L.S., Torres-Peraza, J., Graham, R.K., Watanabe, M.*, et al.* (2013). Suppressing aberrant GluN3A expression rescues synaptic and behavioral impairments in Huntington's disease models. Nat Med *19*, 1030-1038.

Martyn, A.C., Toth, K., Schmalzigaug, R., Hedrick, N.G., Rodriguiz, R.M., Yasuda, R., Wetsel, W.C., and Premont, R.T. (2018). GIT1 regulates synaptic structural plasticity underlying learning. PLoS One *13*, e0194350.

Mueller, H.T., and Meador-Woodruff, J.H. (2004). NR3A NMDA receptor subunit mRNA expression in schizophrenia, depression and bipolar disorder. Schizophrenia research *71*, 361-370.

Murillo, A., Navarro, A.I., Puelles, E., Zhang, Y., Petros, T.J., and Perez-Otano, I. (2021). Temporal Dynamics and Neuronal Specificity of Grin3a Expression in the Mouse Forebrain. Cerebral Cortex *31*, 1914-1926.

Ohi, K., Hashimoto, R., Ikeda, M., Yamamori, H., Yasuda, Y., Fujimoto, M., Umeda-Yano, S., Fukunaga, M., Fujino, H., Watanabe, Y.*, et al.* (2015). Glutamate Networks Implicate Cognitive Impairments in Schizophrenia: Genome-Wide Association Studies of 52 Cognitive Phenotypes. Schizophrenia bulletin *41*, 909-918.

Otsu, Y., Darcq, E., Pietrajtis, K., Matyas, F., Schwartz, E., Bessaih, T., Abi Gerges, S., Rousseau, C.V., Grand, T., Dieudonne, S.*, et al.* (2019). Control of aversion by glycine-gated GluN1/GluN3A NMDA receptors in the adult medial habenula. Science *366*, 250-254.

Paoletti, P., Bellone, C., and Zhou, Q. (2013). NMDA receptor subunit diversity: impact on receptor properties, synaptic plasticity and disease. Nat Rev Neurosci *14*, 383-400.

Papenberg, G., Li, S.C., Nagel, I.E., Nietfeld, W., Schjeide, B.M., Schroder, J., Bertram, L., Heekeren, H.R., Lindenberger, U., and Backman, L. (2014). Dopamine and glutamate receptor genes interactively influence episodic memory in old age. Neurobiology of aging *35*, 1213 e1213-1218.

Perez-Otano, I., Larsen, R.S., and Wesseling, J.F. (2016). Emerging roles of GluN3-containing NMDA receptors in the CNS. Nat Rev Neurosci *17*, 623-635.

Perez-Otano, I., Lujan, R., Tavalin, S.J., Plomann, M., Modregger, J., Liu, X.B., Jones, E.G., Heinemann, S.F., Lo, D.C., and Ehlers, M.D. (2006). Endocytosis and synaptic removal of NR3A-containing NMDA receptors by PACSIN1/syndapin1. Nat Neurosci *9*, 611-621.

Perez-Otano, I., Schulteis, C.T., Contractor, A., Lipton, S.A., Trimmer, J.S., Sucher, N.J., and Heinemann, S.F. (2001). Assembly with the NR1 subunit is required for surface expression of NR3A-containing NMDA receptors. J Neurosci *21*, 1228-1237.

Poulopoulos, A., Murphy, A.J., Ozkan, A., Davis, P., Hatch, J., Kirchner, R., and Macklis, J.D. (2019). Subcellular transcriptomes and proteomes of developing axon projections in the cerebral cortex. Nature *565*, 356-360.

Rao, V.R., Pintchovski, S.A., Chin, J., Peebles, C.L., Mitra, S., and Finkbeiner, S. (2006). AMPA receptors regulate transcription of the plasticity-related immediate-early gene Arc. Nat Neurosci *9*, 887-895.

Redondo, R.L., and Morris, R.G. (2011). Making memories last: the synaptic tagging and capture hypothesis. Nat Rev Neurosci *12*, 17-30.

Roberts, A.C., Diez-Garcia, J., Rodriguiz, R.M., Lopez, I.P., Lujan, R., Martinez-Turrillas, R., Pico, E., Henson, M.A., Bernardo, D.R., Jarrett, T.M.*, et al.* (2009). Downregulation of NR3A-containing NMDARs is required for synapse maturation and memory consolidation. Neuron *63*, 342-356.

Sadat-Shirazi, M.S., Ashabi, G., Hessari, M.B., Khalifeh, S., Neirizi, N.M., Matloub, M., Safarzadeh, M., Vousooghi, N., and Zarrindast, M.R. (2019). NMDA receptors of blood lymphocytes anticipate cognitive performance variations in healthy volunteers. Physiology & behavior *201*, 53-58.

Sancak, Y., Bar-Peled, L., Zoncu, R., Markhard, A.L., Nada, S., and Sabatini, D.M. (2010). Ragulator-Rag complex targets mTORC1 to the lysosomal surface and is necessary for its activation by amino acids. Cell *141*, 290-303.

Santini, E., Huynh, T.N., MacAskill, A.F., Carter, A.G., Pierre, P., Ruggero, D., Kaphzan, H., and Klann, E. (2013). Exaggerated translation causes synaptic and behavioural aberrations associated with autism. Nature *493*, 411-415.

Sarker, G., Sun, W., Rosenkranz, D., Pelczar, P., Opitz, L., Efthymiou, V., Wolfrum, C., and Peleg-Raibstein, D. (2019). Maternal overnutrition programs hedonic and metabolic phenotypes across generations through sperm tsRNAs. Proc Natl Acad Sci U S A *116*, 10547-10556.

Sharma, V., Sood, R., Khlaifia, A., Eslamizade, M.J., Hung, T.Y., Lou, D., Asgarihafshejani, A., Lalzar, M., Kiniry, S.J., Stokes, M.P.*, et al.* (2020). eIF2alpha controls memory consolidation via excitatory and somatostatin neurons. Nature *586*, 412-416.

Shrestha, P., Ayata, P., Herrero-Vidal, P., Longo, F., Gastone, A., LeDoux, J.E., Heintz, N., and Klann, E. (2020a). Cell-type-specific drug-inducible protein synthesis inhibition demonstrates that memory consolidation requires rapid neuronal translation. Nat Neurosci *23*, 281-292.

Shrestha, P., Shan, Z., Mamcarz, M., Ruiz, K.S.A., Zerihoun, A.T., Juan, C.Y., Herrero-Vidal, P.M., Pelletier, J., Heintz, N., and Klann, E. (2020b). Amygdala inhibitory neurons as loci for translation in emotional memories. Nature *586*, 407-411.

Smithson, L.J., and Gutmann, D.H. (2016). Proteomic analysis reveals GIT1 as a novel mTOR complex component critical for mediating astrocyte survival. Genes & development *30*, 1383-1388.

Sossin, W.S., and Costa-Mattioli, M. (2019). Translational Control in the Brain in Health and Disease. Cold Spring Harbor perspectives in biology.

Stern, E., Chinnakkaruppan, A., David, O., Sonenberg, N., and Rosenblum, K. (2013). Blocking the eIF2alpha kinase (PKR) enhances positive and negative forms of cortex-dependent taste memory. J Neurosci *33*, 2517-2525.

Stoica, L., Zhu, P.J., Huang, W., Zhou, H., Kozma, S.C., and Costa-Mattioli, M. (2011). Selective pharmacogenetic inhibition of mammalian target of Rapamycin complex I (mTORC1) blocks long-term synaptic plasticity and memory storage. Proc Natl Acad Sci U S A *108*, 3791-3796.

Takata, A., Iwayama, Y., Fukuo, Y., Ikeda, M., Okochi, T., Maekawa, M., Toyota, T., Yamada, K., Hattori, E., Ohnishi, T.*, et al.* (2013). A population-specific uncommon variant in GRIN3A associated with schizophrenia. Biol Psychiatry *73*, 532-539.

Takei, N., Inamura, N., Kawamura, M., Namba, H., Hara, K., Yonezawa, K., and Nawa, H. (2004). Brain-derived neurotrophic factor induces mammalian target of rapamycin-dependent local activation of translation machinery and protein synthesis in neuronal dendrites. J Neurosci *24*, 9760-9769.

Tang, S.J., Reis, G., Kang, H., Gingras, A.C., Sonenberg, N., and Schuman, E.M. (2002). A rapamycin-sensitive signaling pathway contributes to long-term synaptic plasticity in the hippocampus. Proc Natl Acad Sci U S A *99*, 467-472.

Trinh, M.A., Kaphzan, H., Wek, R.C., Pierre, P., Cavener, D.R., and Klann, E. (2012). Brain-specific disruption of the eIF2alpha kinase PERK decreases ATF4 expression and impairs behavioral flexibility. Cell Rep *1*, 676-688.

Wang, C.C., Held, R.G., Chang, S.C., Yang, L., Delpire, E., Ghosh, A., and Hall, B.J. (2011). A critical role for GluN2B-containing NMDA receptors in cortical development and function. Neuron *72*, 789-805.

Wang, D.O., Martin, K.C., and Zukin, R.S. (2010). Spatially restricting gene expression by local translation at synapses. Trends in neurosciences *33*, 173-182.

Won, H., Mah, W., Kim, E., Kim, J.W., Hahm, E.K., Kim, M.H., Cho, S., Kim, J., Jang, H., Cho, S.C.*, et al.* (2011). GIT1 is associated with ADHD in humans and ADHD-like behaviors in mice. Nat Med *17*, 566-572.

Yang, J., Wang, S., Yang, Z., Hodgkinson, C.A., Iarikova, P., Ma, J.Z., Payne, T.J., Goldman, D., and Li, M.D. (2015). The contribution of rare and common variants in 30 genes to risk nicotine dependence. Mol Psychiatry *20*, 1467-1478.

Yap, E.L., and Greenberg, M.E. (2018). Activity-Regulated Transcription: Bridging the Gap between Neural Activity and Behavior. Neuron *100*, 330-348.

Yuan, T., Mameli, M., O'Connor, E.C., Dey, P.N., Verpelli, C., Sala, C., Perez-Otano, I., Luscher, C., and Bellone, C. (2013). Expression of cocaine-evoked synaptic plasticity by GluN3A-containing NMDA receptors. Neuron *80*, 1025-1038.

Zhang, H., Webb, D.J., Asmussen, H., and Horwitz, A.F. (2003). Synapse formation is regulated by the signaling adaptor GIT1. The Journal of cell biology *161*, 131-142.

Zhu, P.J., Chen, C.J., Mays, J., Stoica, L., and Costa-Mattioli, M. (2018). mTORC2, but not mTORC1, is required for hippocampal mGluR-LTD and associated behaviors. Nat Neurosci *21*, 799-802.

SUPPLEMENTAL INFORMATION

Control of protein synthesis and memory by GluN3A-NMDA receptors through inhibition of GIT1/mTORC1 assembly

Supplemental information includes nine figures and two Key Resources Tables.

Supplemental Figures

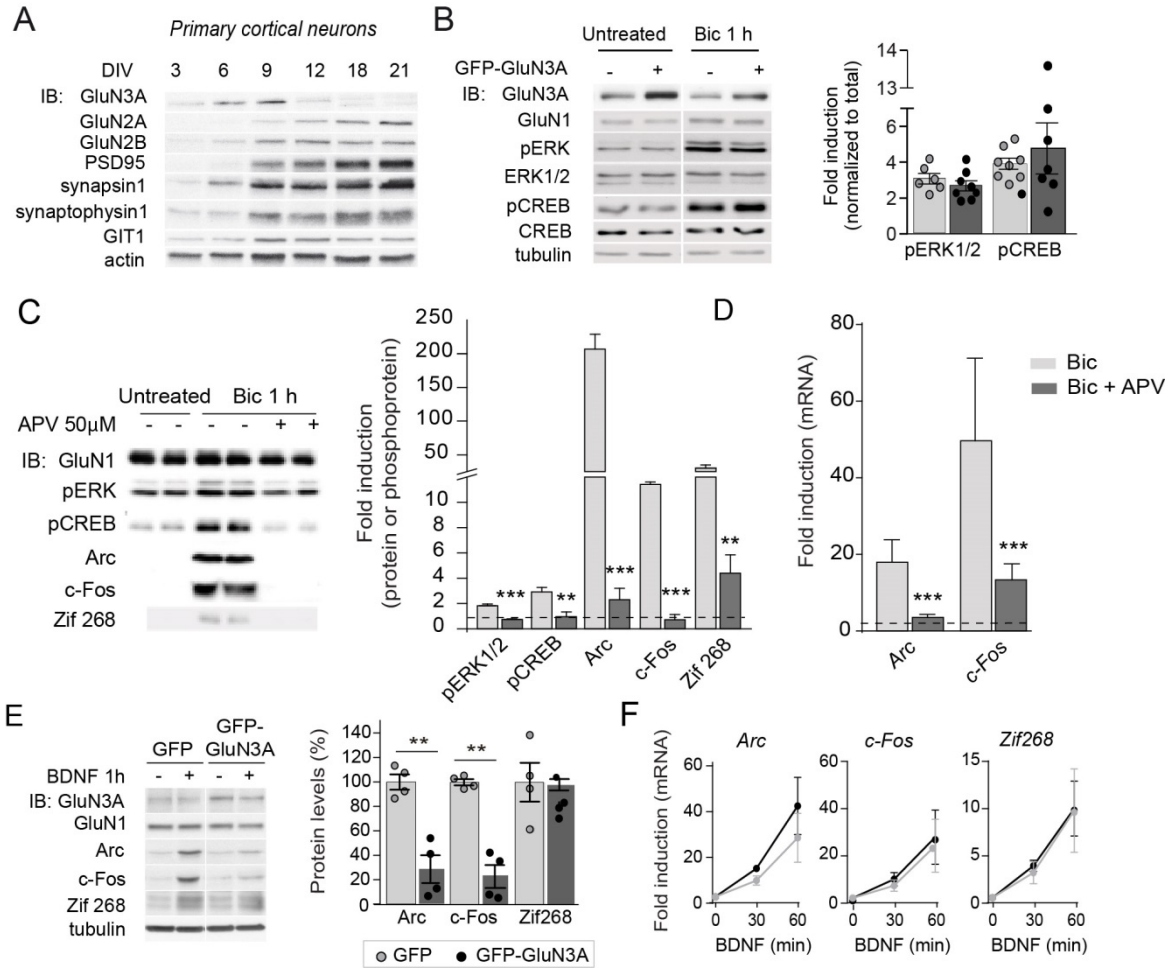

Figure 1 – figure supplement 1. Selective *versus* global effects of GluN3A expression and general NMDAR blockade on activity-dependent signaling

(**A**) Immunoblot (IB) analysis of the time-course of expression of NMDAR subunits and a repertoire of synaptic proteins in cultured cortical neurons. (**B**) Immunoblot analysis of ERK1/2 and CREB phosphorylation in whole cell lysates of DIV14 cortical neurons treated with bicuculline for 1 h. Left, representative western blots probed with the indicated antibodies. Right, fold-induction by bicuculline of phosphorylated proteins normalized to their total levels (n=6-8 from 3-4 independent cultures). (**C**) Total lysates from cortical neurons pretreated with APV (50 µM, 30 min) before stimulation with bicuculline (50 µM, 1 h) were immunoblotted with the indicated antibodies. Quantification showed a general blockade of activity dependent by APV (n=4-6 samples from 2-3 independent cultures, **p<0.01, ***p<0.001 ANOVA followed by Tukey´s test). (**D**) APV blocked the increase in *Arc* and *c-Fos* mRNA induced by bicuculline (n=6-10 samples from 3 independent cultures, ***p<0.001 one-way ANOVA followed by Tukey´s test). Data are expressed as fold-induction of non-stimulated neurons. (**E, F**) Analogous experiments to the ones in Figure 1B, C were conducted upon stimulation with BDNF (100 ng/ml, 1 h).

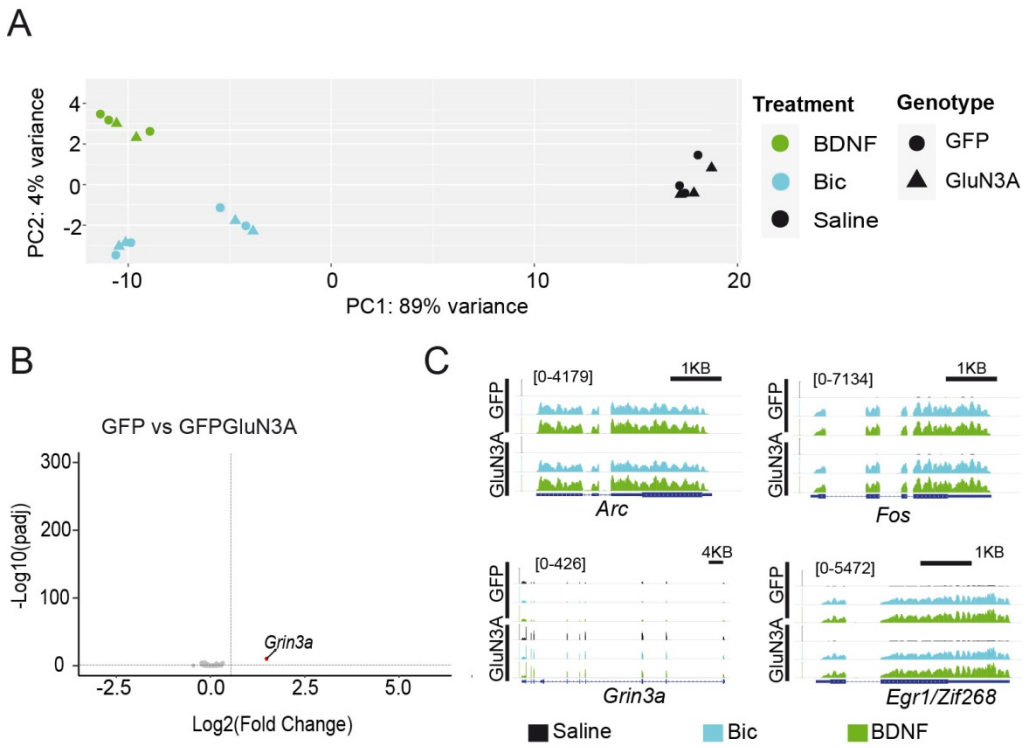

Figure 1 – figure supplement 2. RNAseq analysis of activity-dependent gene expression

(**A**) Principal Component Analysis plot representing all RNAseq samples. (**B**) Volcano plot from RNAseq analysis from gene expression in untreated DIV14 neurons infected with GFP or GFP-GluN3A. (**C**) Integrative Genome Viewer (IGV) tracks for RNAseq signal at representative genes in the different conditions. The IEGs *Arc*, *c-Fos* and *Egr1* are similarly induced by bicuculline (Bic) and BDNF treatments in GFP and GFP-GluN3a-transduced cultures. Note that levels of *Grin3a* are very much increased in GFP-GluN3A-transduced cultures compared to GFP-transduced cultures.

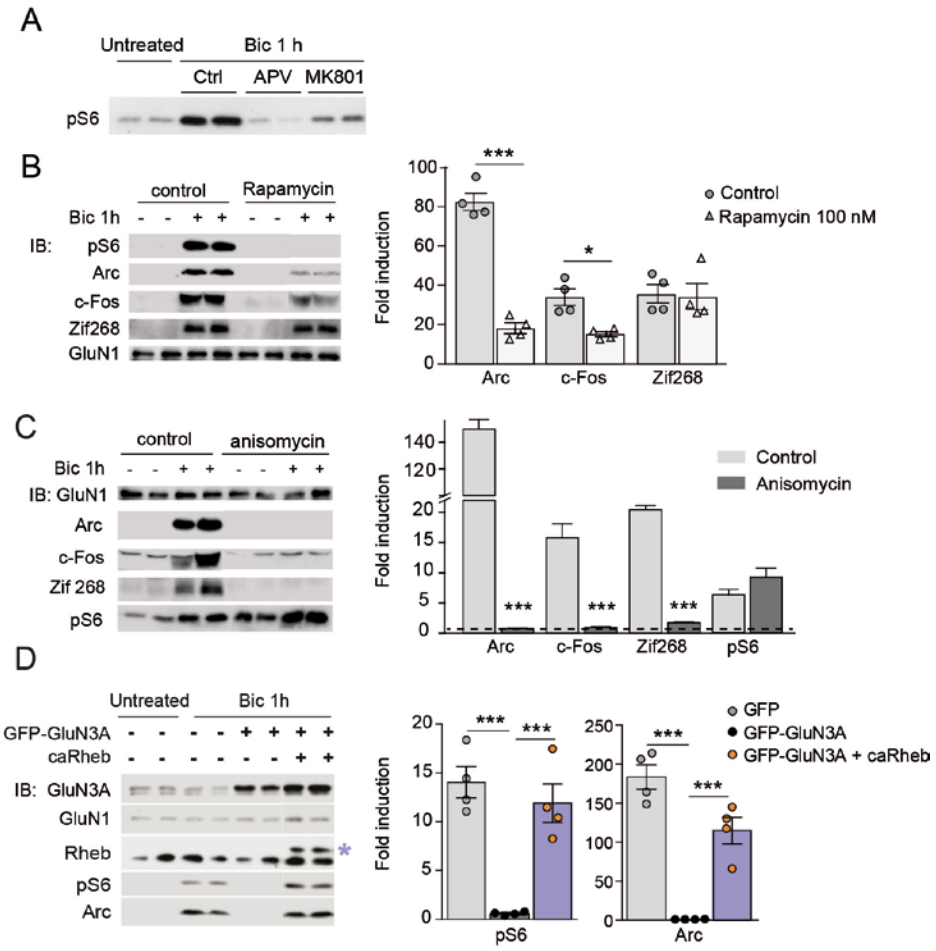

Figure 2 – figure supplement 1. Selective mTORC1-dependence of IEG translation

(A) Immunoblot analysis of the phosphorylation status of the mTOR downstream effector S6 in lysates from DIV14 cortical neurons stimulated with bicuculline in the absence (Ctrl) or presence of APV (50 µM, 30 min) or MK801 (10 µM, 1 h). **(B)** mTORC1 signaling is required for activity-dependent induction of Arc and c-Fos but not Zif268. Left, representative western blots of DIV14 neurons stimulated with bicuculline after pre-incubation with rapamycin (100 nM, 1 h before and during bicuculline treatment). Right, fold-induction of IEGs in response to bicuculline (n=4 from 2 independent cultures; *p<0.05, ***p<0.001, two-tailed paired t-test). (**C**) General inhibition of protein synthesis blocks activity-induction of Arc, c-Fos and Zif268. Whole lysates from DIV14 cortical neurons either untreated or treated with bicuculline (50 µM, 1 h) and anisomycin (0.8 µM, 1 h) were immunoblotted with the indicated antibodies. Left, representative immunoblots and right, quantifications, show a general blockade of IEGs tested by anisomycin. Data are expressed as fold-induction of non-treated neurons (n=3-4 independent cultures, ***p<0.001 ANOVA followed by Tukey´s test). **(D)** Reactivation of mTOR in GFP-GluN3A infected neurons by AAV-driven constitutively active Rheb (caRheb) rescues Arc induction. Left, representative western blots of neurons infected with lentiviral GFP-GluN3A and AAV-caRheb and treated with bicuculline. Right, fold-induction by bicuculline of pS6 and Arc in the indicated conditions (n=4 from 2 independent cultures; ***p<0.001, one-way ANOVA followed by Tukey's test).

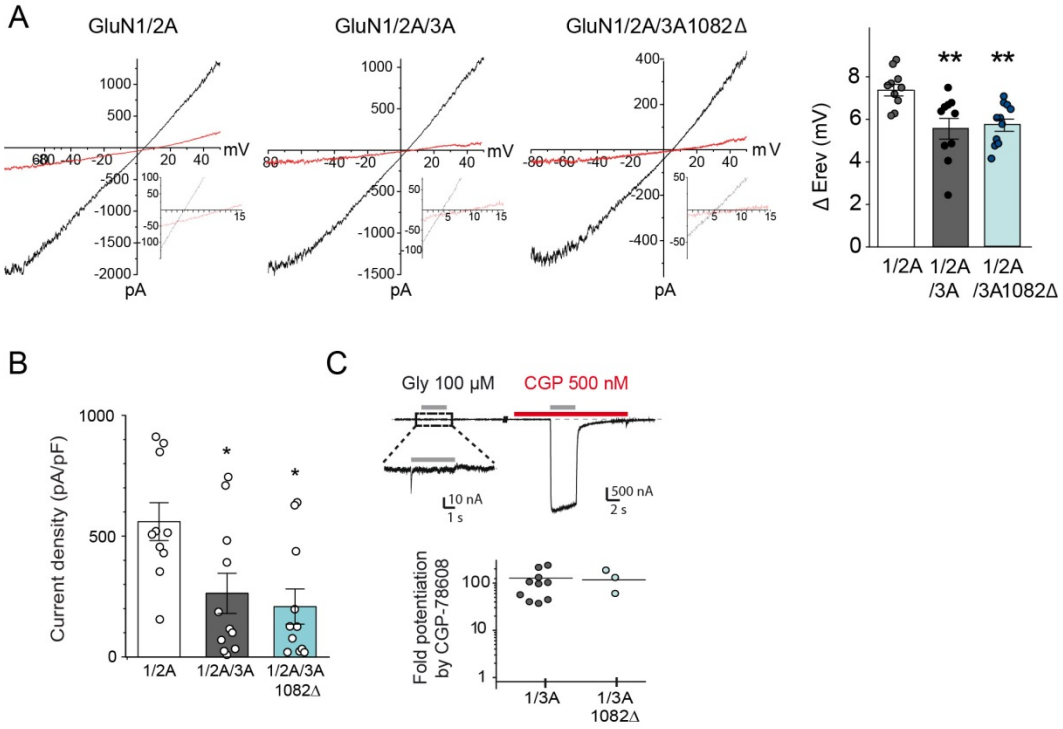

Figure 3 – figure supplement 1. Electrophysiological properties of recombinant NMDA and excitatory glycine receptors containing full-length or truncated GluN3A

(**A**) Left, representative steady-state glutamate-evoked ramp currents obtained with 2 mM (black) and 10 mM (red) extracellular Ca2+ for HEK293 cells expressing GluN1A/GluN2A alone, or with either GFP-GluN3A or GFP-GluN3A1082Δ. Insets show currents on expanded scale to highlight the Erev. Right, summary graph of the ΔErev obtained from multiple experiments is shown on right (n=10–11, **p<0.01, one-way ANOVA followed by Bonferroni post-hoc test). (**B**) Summary graph depicting current density from HEK293 cells expressing GluN1A/GluN2A alone, or with either GFP-GluN3A or GFP-GluN3A1082Δ (*p<0.05 compared to GluN1A/GluN2A, one-way ANOVA followed by Bonferroni post-hoc test). (**C**) Top, responses to glycine of HEK293 cells expressing GluN1/GluN3A receptors in absence or presence of CGP-78608 (500 nM). Bottom, quantification of fold peak current potentiation by CGP-78608 for GluN1/GluN3A and GluN1/GluN3A1082Δ receptors (n=3-11).

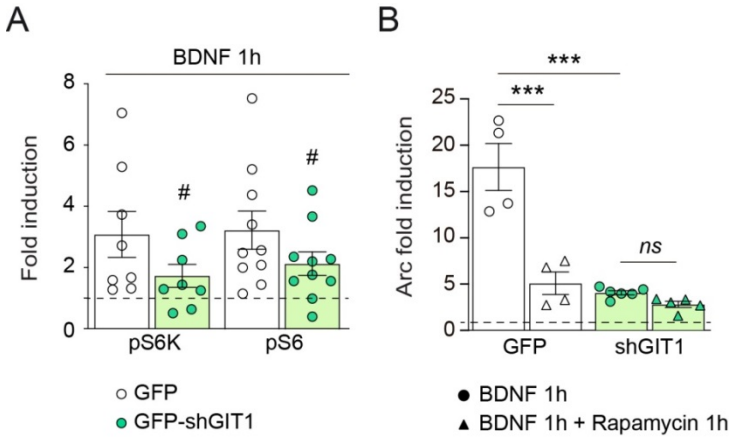

Figure 4 – figure supplement 1. GIT1 knockdown reduces mTORC1 activation by BDNF and rapamycin-sensitive Arc translation

Cortical neurons infected with lentivirus expressing a shRNA against GIT1 (GFP-shGIT1) or a control lentivirus (GFP) were stimulated with BDNF (100 ng/ml, 1 h) with or without pre-incubation with rapamycin (100 nM, 1h). (**A**) BDNF induction of phosphorylated S6K and S6 normalized to total protein levels (n=8-10 samples from 4-5 independent cultures; # pS6K: p=0.13, # pS6: p=0.05, two-tailed paired t-test). (**B**) Induction by BDNF of Arc protein (n=4-6 samples from 2 independent cultures; ***p<0.001, two-way ANOVA followed by Tukey's test).

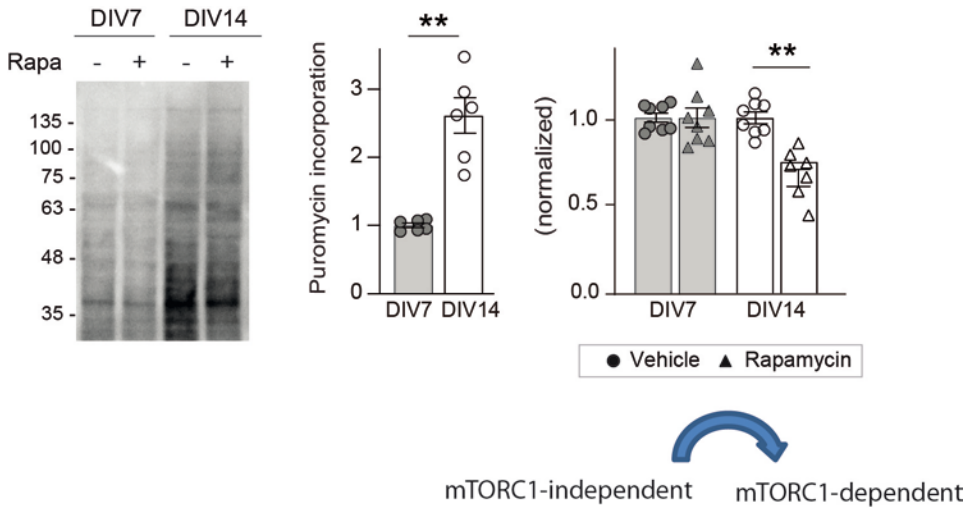

Figure 5 – figure supplement 1. Age-dependent emergence of mTORC1-dependent protein synthesis in cortical neurons

Representative blots and quantification of puromycin incorporation in the presence or absence of 100 nM rapamycin in wild-type DIV7 and DIV14 neurons. Puromycin levels were normalized to Ponceau S staining (n=6-8 samples from 3-4 independent cultures; **p<0.01, followed by Tukey's test).

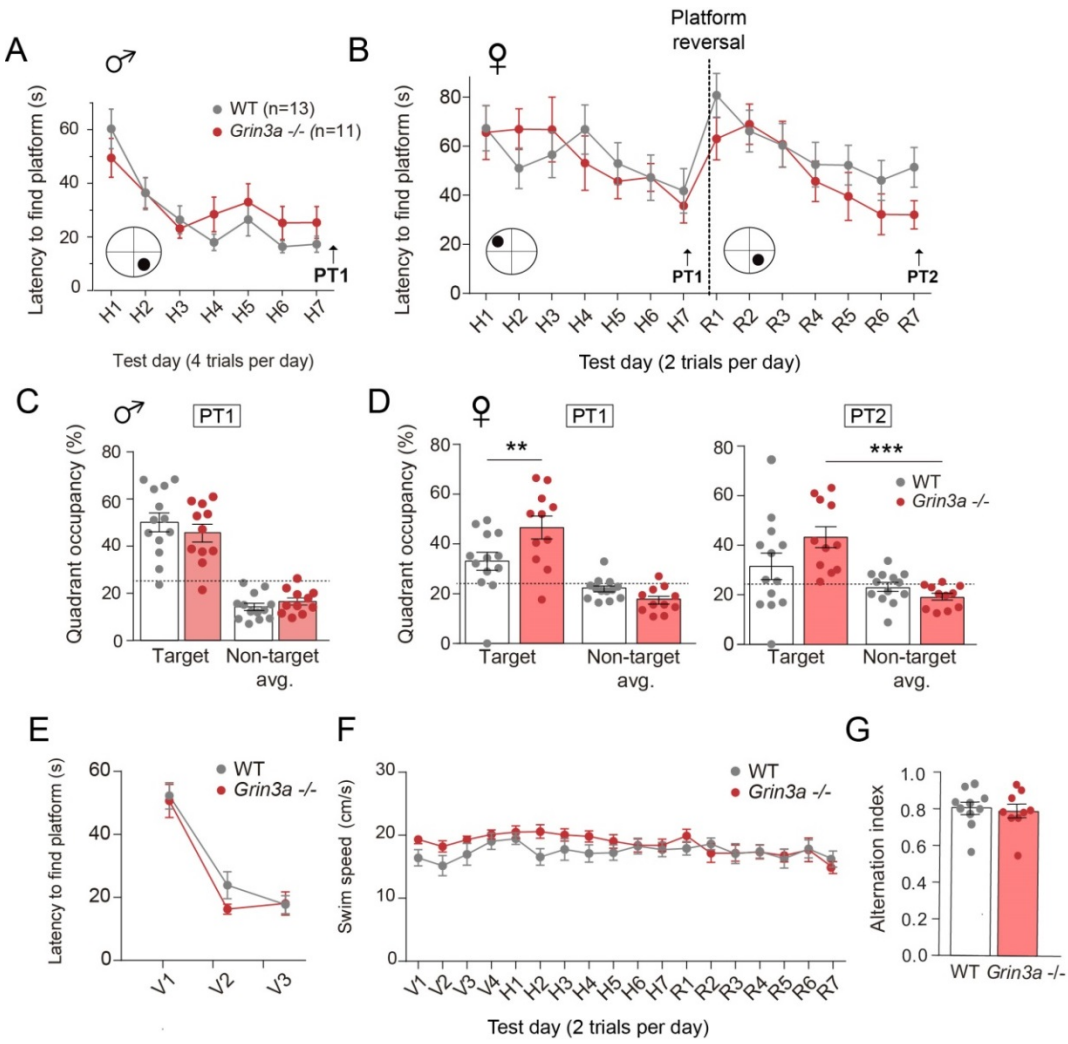

Figure 6 – figure supplement 1. Behavior of male and female *Grin3a-/-* mice in the Morris Water Maze

(**A**) Escape latencies of male wild-type (WT) and *Grin3a -/-* mice over the time-course of training on a standard hidden-platform version of the Morris water maze (7 days, 4 trials per day). (**B**) Escape latencies of female *Grin3a -/-* and WT mice over the course of training (2 trials per day). (**C**) On probe trials for memory acquisition performed 24 hours after day 7 (PT1), both groups showed similar preference for the target quadrant (n=11-13 mice per group). Dashed lines indicate chance levels (25%). (**D**) Left, On the probe test performed 24 hours after day 7 (PT1), female *Grin3a -/-* mice showed enhanced preference for the target quadrant relative to WT (n=11-13 mice per group; 2-way ANOVA with Bonferroni post-hoc test; p=0.0062). Right, on probe tests 24 hours after completion of reversal training (PT2), female *Grin3a-/-* showed significant preference for the target quadrant (n=11-13 mice per genotype; two-way ANOVA with Bonferroni *post-hoc* test, ***p<0.0001). (**E**) WT and *Grin3a -/-* mice showed no differences in times to reach a visible platform. (**F**) Swimming speed over the training period. Data plotted correspond to the experiment shown in Fig. 7C. (**G**) Alternation index of wild-type (WT) *and Grin3a-/-* mice in the Y-maze (n=9-10 mice per genotype).

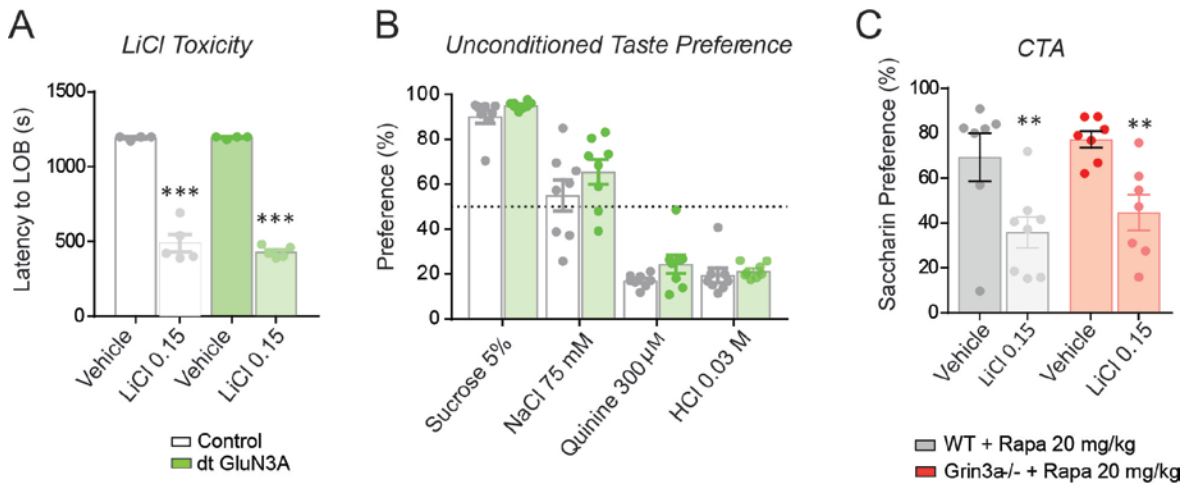

Figure 6 – figure supplement 2. Controls for conditioned taste aversion (CTA) experiments

(**A**) Double transgenic GluN3A (dtGluN3A) and WT mice showed similar "lying on belly" latencies after a 0.15 M LiCl injection (n=4-5 mice per group; unpaired two-tailed t-test, ***p<0.001). (**B**) dt-GluN3A and control mice showed similar taste preferences (n=8 mice per group). (**C**) The rapamycin treatment regime used does not impair the formation of "standard" CTA memory in WT nor *Grin3a-/-* mice (n=6-8 mice per group; 2-way ANOVA with Bonferroni post-hoc test, **p<0.01).

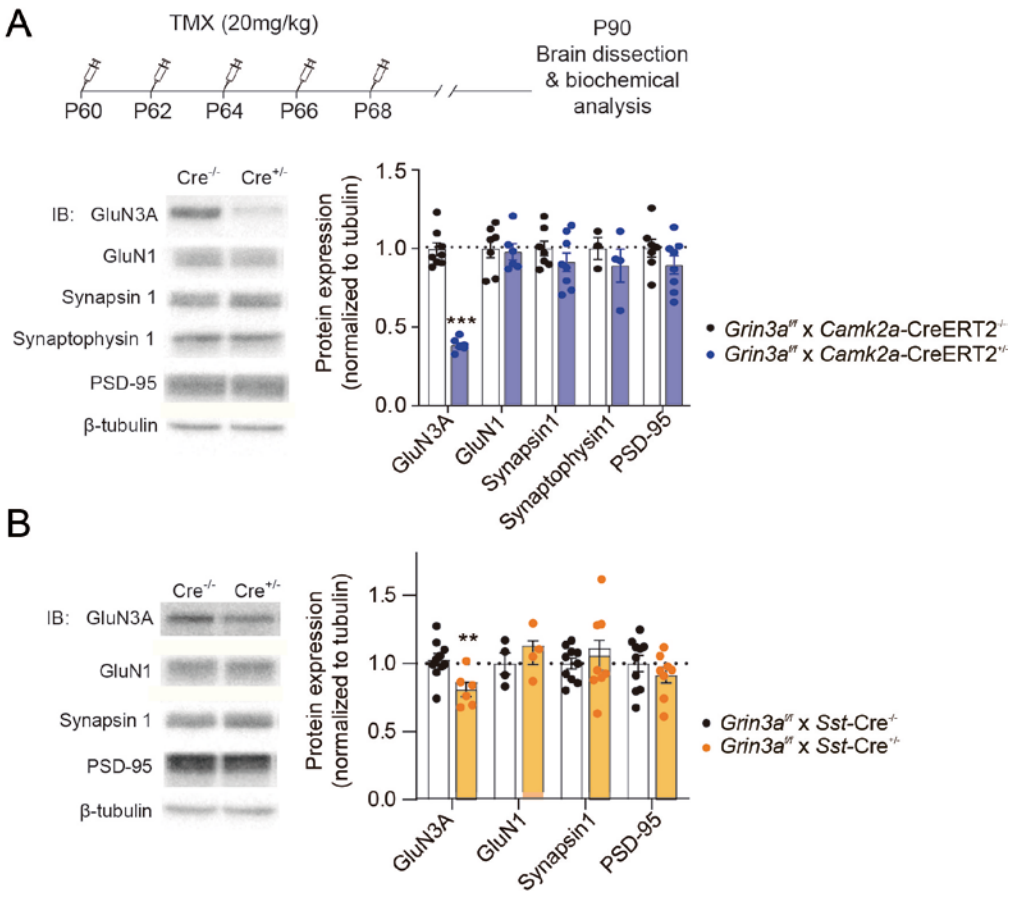

Figure 7 – figure supplement 1. Expression of GluN3A and other synaptic proteins in conditional *Grin3a* knockout mice

(**A**) Top, tamoxifen (TMX) administration regime to *Grin3a*$^{f/f}$ x *CamK2a*-CreER^{T2} mice. Hippocampal lysates of P90 mice were analyzed by SDS-PAGE and immunoblotted for the indicated proteins (n=4-8 mice per group; unpaired two-tailed t-test, ***p<0.0001). (**B**) Immunoblot analysis of hippocampal lysates of P90 *Grin3a*$^{f/f}$ x *Som*-Cre mice (n=4-10 mice per group; unpaired two-tailed t-test, **p<0.01). Note that conditional deletion of Grin3a decreases GluN3A expression without affecting other synaptic proteins.

KEY RESOURCES TABLES

Table S1. Primers used in qPCR analysis

Primer	Host	Sequence (5' – 3')	Fragment size
Arc_Fwd	Mo	GAGCCTACAGAGCCAGGAGA	340bp
Arc_Rv	Mo	TGCCTTGAAAGTGTCTTGGA	
c-Fos_fwd	Mo/ Rat	CTGCTCTACTTTGCCCCTTCT	215bp
c-Fos_rv	Mo/ Rat	TTTATCCCCACGGTGACAGC	
GAPDH_fwd	Mo/ Rat	CATGGCCTTCCGTGTTCCT	85bp
GAPDH_rv	Mo/ Rat	TGATGTCATCATACTTGGCAGGTT	
Zif268_fwd	Mo/ Rat	AGAAGCCTTTTGCCTGTGACA	54bp
Zif268_rv	Mo/ Rat	CGTTCATCACTCCTGGCAAAC	

Table S2. Primary antibodies used for biochemistry and imaging.

Antibody	Source	Identifier
Arc (clone C-7) mouse monoclonal; WB 1:100	Santa Cruz Biotechnology	Cat# sc-17839; RRID: AB_626696
BetaPix, SH3 domain rabbit polyclonal; WB 1:1000	Millipore	Cat# 07-1450; RRID: AB_1586904
Beta-Tubulin III mouse monoclonal; WB 1:20000	Sigma-Aldrich	Cat# T8660; RRID: AB_477590
c-Fos (4) rabbit polyclonal; WB 1:500	Santa Cruz Biotechnology	Cat# sc-52; RRID: AB_2106783
CREB (clone 48H2) rabbit monoclonal; WB 1:1000	Cell Signaling	Cat# 9197; RRID: AB_331277
Egr-1/ Zif268 (clone 588) rabbit monoclonal; WB 1:500	Santa Cruz Biotechnology	Cat# sc-110; RRID: AB_2097174
GIT1 (A-1) mouse monoclonal; PLA 1:150	Santa Cruz Biotechnology	Cat# sc-365084; RRID: AB_10850059
GIT1 rabbit polyclonal; IP 1:200, WB 1:1000	Cell Signaling	Cat# 2919; RRID: AB_2109982
mTOR rabbit polyclonal; IP 1:100, PLA 1:150, WB 1:1000	Cell Signaling	Cat# 2972; RRID: AB_330978
NMDAR1, all splice variants (clone R1JHL) mouse monoclonal; WB 1:1000	Millipore	Cat# MAB1586; RRID: AB_11213180
NMDAR2A&B, pan antibody rabbit polyclonal; WB 1:1000	Millipore	Cat# AB1548; RRID: AB_11212156
NR2A (clone A12W) rabbit monoclonal; WB 1:1000	Millipore	Cat# 05-901R; RRID: AB_10805961
NR2B (clone BWJHL) mouse monoclonal; WB 1:1000	Millipore	Cat# 05-920; RRID: AB_417391
NR3A mouse monoclonal; WB 1:100	Gift of Jim Trimmer (UCDavis)	N/A
NR3A rabbit polyclonal; WB 1:1000	Millipore	Cat# 07-356; RRID: AB_2112620
p44/42 MAPK (Erk1/2) rabbit polyclonal; WB 1:1000	Cell Signaling	Cat# 9102; RRID: AB_330744
p70 S6 kinase rabbit polyclonal; WB 1:1000	Cell Signaling	Cat# 9202; RRID: AB_331676
Phospho-CREB Ser133 rabbit polyclonal; WB 1:1000	Millipore	Cat# 06-519; RRID: AB_310153
Phospho-mTOR Ser2448 rabbit polyclonal;	Cell Signaling	Cat# 2971; RRID: AB_330970

WB 1:1000		
Phospho-p44/42 MAPK (Erk1/2) Thr202/Tyr204 rabbit polyclonal; WB 1:1000	Cell Signaling	Cat# 9101; RRID: AB_331646
Phospho-p70 S6 kinase Thr389 (clone 108D2) rabbit monoclonal; WB 1:1000	Cell Signaling	Cat# 9234; RRID: AB_2269803
Phospho-S6 ribosomal protein Ser240/244 rabbit polyclonal; WB 1:1000	Cell Signaling	Cat# 2215; RRID: AB_331682
PSD-95 mouse monoclonal WB 1:1000	Antibodies Incorporated	Cat# 75-028 RRID: AB_10698024
Puromycin (clone 12D10) mouse monoclonal; WB 1:2000	Millipore	Cat# MABE343; RRID: AB_2566826
Raptor (clone 24C12) rabbit monoclonal; WB 1:1000	Cell Signaling	Cat# 2280; RRID: AB_561245
Rheb (clone E1G1R) rabbit monoclonal; WB 1:1000	Cell Signaling	Cat# 13879; RRID: AB_2721022
Rictor rabbit polyclonal; WB 1:1000	Cell Signaling	Cat# 2140; RRID: AB_ 2179961
S6 ribosomal protein (clone 5G10) rabbit monoclonal; WB 1:1000	Cell Signaling	Cat# 2217; RRID: AB_331355
Synapsin I mouse monoclonal WB 1:5000	Synaptic Systems	Cat# 106 011 RRID: AB_2619772
Synaptophysin (clone SY38) mouse monoclonal; WB 1:2000	Millipore	Cat# MAB5258; RRID: AB_11214133

Supplemental references

Software used for bioinformatics analysis

https://www.bioinformatics.babraham.ac.uk/projects/trim_galore/

https://pubmed.ncbi.nlm.nih.gov/23104886/

https://pubmed.ncbi.nlm.nih.gov/19505943/

https://pubmed.ncbi.nlm.nih.gov/19617889/

https://academic.oup.com/bib/article/14/2/178/208453

https://pubmed.ncbi.nlm.nih.gov/25516281/

https://academic.oup.com/nar/article/47/8/e47/5345150

https://academic.oup.com/nar/article/43/7/e47/2414268

https://academic.oup.com/nar/article/44/W1/W160/2499308

https://github.com/kevinblighe/EnhancedVolcano